# FUSE Spectroscopy of the White Dwarf in U Geminorum<sup>1</sup>

Knox S. Long

long@stsci.edu

Space Telescope Science Institute, 3700 San Martin Drive, Baltimore, MD 21218

Gabriel Brammer

gabriel.brammer@yale.edu

Department of Astronomy, Yale University, New Haven, CT, 06520

and

Cynthia S. Froning

cfroning@casa.colorado.edu

Center for Astrophysics and Space Astronomy, University of Colorado, 593 UCB, Boulder, CO, 80309

### ABSTRACT

Observations of U Gem with FUSE confirm that the WD is heated by the outburst and cools during quiescence. At the end of an outburst, the best uniform temperature WD model fits to the data indicate a temperature of 41,000 - 47,000 K, while in mid-quiescence, the temperature is 28,000 - 31,000 K, depending on the gravity assumed for the WD. Photospheric abundance patterns at the end of the outburst and in mid-quiescence show evidence of CNO processing. Improved fits to the spectra can be obtained assuming there is a hotter, heated portion of the WD, presumably an accretion belt, with a temperature of 60,000 - 70,000 K occupying 14-32% of the surface immediately after outburst. However, other relatively simple models for the second component fit the data just as well and there is no obvious signature that supports the hypothesis that the second component arises from a separate region of the WD surface. Hence, other physical explanations still must be considered to explain the time evolution of the spectrum of U Gem in quiescence. Strong orbital phase dependent absorption, most likely due to gas above the disk, was observed during the mid-quiescence spectrum. This

material, which can be modeled in terms of gas with a temperature of 10,000-11,000 K and a density of  $10^{13}$  cm<sup>-3</sup>, has a column density of  $\sim 2 \times 10^{21}$  cm<sup>-2</sup> at orbital phase 0.6-0.85, and is probably the same material that has been observed to cause dips in the lightcurve at X-ray wavelengths in the past. The discrepancy described by Naylor et al. (2005) between the radius of the WD derived on the one hand by the UV spectral analysis and the distance to U Gem, and on the other, by the orbital elements and the gravitational redshift remains a serious problem.

Subject headings: accretion, accretion disks — binaries: close — stars: mass-loss — novae, cataclysmic variables — stars: individual (U Geminorum)

#### 1. Introduction

Dwarf novae (DNe) are binary star systems that undergo semi-regular outbursts in which the system brightens by 3-5 visual magnitudes. DNe consist of a white dwarf (WD) surrounded by an accretion disk of material transferred from a low-mass late-type companion star. The outbursts are triggered by a thermal instability in the disk that causes an increase in the mass transfer rate (Hōshi 1979; Mineshige & Osaki 1983) and can last from a day to several weeks. In outburst, the disk is hot, ionized and optically thick and is the dominant source of UV and optical emission. In quiescence the disk is cool, mostly neutral, and optically thin in the continuum, and the ultraviolet (UV) flux is usually, but not always, dominated by emission from the WD. DNe are members of the larger class of cataclysmic variables (CVs), all of which contain a mass-accreting WD and whose properties are significantly affected by the magnetic field of the WD. In DNe, the strength of the field is sufficiently low for an accretion disk to form and extend (close) to the WD.

U Gem was the first cataclysmic variable (CV) and the first DN discovered, and as such, is regarded as the prototypical DN. U Gem undergoes outbursts lasting typically 7-14 days of about 5 magnitudes, reaching a peak magnitude of 9.1 about 3 times a year (Szkody & Mattei 1984). There are two types of outbursts, narrow and wide, lasting  $\sim$ 7 and  $\sim$ 14 days, respectively (Ak et al. 2002). Unlike some prototypes, it remains a reasonable prototype for other DNe. The WD in the system is fairly massive, 1.1  $M_{\odot}$  (Sion et al. 1998; Long & Gilliland 1999), and hot, 30,000 K in mid-quiescence (Panek & Holm 1984; Kiplinger et al.

<sup>&</sup>lt;sup>1</sup>Based on observations made with the NASA-CNES-CSA Far Ultraviolet Spectroscopic Explorer. FUSE is operated for NASA by the Johns Hopkins University under NASA contract NAS5-32985

1991; Long et al. 1993), and does dominate the UV spectrum in quiescence. The UV spectrum in outburst resembles that of a steady state accretion disk with  $\dot{m}$  of  $7 \times 10^{-9}~M_{\odot}~\rm yr^{-1}$  (Panek & Holm 1984; Froning et al. 2001) at the astrometrically determined distance of  $100.4\pm3.7~\rm pc$  (Harrison et al. 2004). During outburst the luminosities of the boundary layer and the disk are similar (Long et al. 1996), as predicted by the standard theory of disk accretion in CVs (Lynden-Bell & Pringle 1974).

IUE observations of a deepening Lyman  $\alpha$  profile and decreasing UV flux provided the first evidence that the WD in U Gem cools between outbursts (Kiplinger et al. 1991). However, the flux decline is less than would occur if the entire WD cooled, and this led Long et al. (1993) to interpret the Hopkins Ultraviolet Telescope spectrum of U Gem, the first spectrum of U Gem in quiescence that extended to the Lyman limit, in terms of a WD with 85% of the surface at 30,000 K and 15% at 57,000 K. They suggested that the hot portion of the WD might either be due to the existence of an accretion belt left over from the outburst that had been predicted by Kippenhahn & Thomas (1978), or possibly due to an elevated accretion rate in the disk plane following the outburst. Subsequent HST observations have tended to confirm the observational facts. The overall spectral shape in the wavelength range 1150-1750 Å and the character of both the Lyman  $\alpha$  absorption profile and the depth of the metal absorption lines seen as a result of on-going accretion resemble that of a 38,000 K WD just after outburst cooling to 30,000 K far from outburst, but the flux evolution implies that there must be at least two components to the spectrum (Long et al. 1994). However, the exact nature of the second component is still unclear.

In principle, observations of U Gem with FUSE can shed light on this problem, both because the hotter component should be more important in the FUSE spectral range 900-1187 A than in the HST range, and because FUSE has sufficient spectral resolution (R $\sim$ 12,500) to separate a slowly rotating WD from a rapidly rotating accretion belt. Here we analyze two observations of U Gem obtained with FUSE, the first, originally described by Froning et al. (2001), at the end of an outburst of U Gem, and the second during mid-quiescence, which we obtained from the FUSE archive and has not to our knowledge been analyzed. Our primary purpose was to better understand the processes that cause the evolution of the spectrum of U Gem in quiescence, and especially of the second component in the spectrum. The remainder of the paper is organized as follows: In Sec. 2, we describe the observations, our reduction of the data, and provide a qualitative description of the spectra that were obtained. In Sec. 3, we analyze the data in terms of WD models, explore the likely elemental abundances in the photosphere of the WD, and try to characterize the nature of the second component in light of complicating evidence of phase-dependent temporal variations in the quiescent FUSE spectra. In Sec. 4, we attempt to synthesize the results in terms of our general understanding of the UV properties of DNe in quiescence and explore a specific discrepancy with the WD radius inferred by different techniques. Finally, in Sec. 5, we sum up.

# 2. Observations and Data Reduction

As indicated in Fig. 1, both of the observations described here occurred when system was in optical quiescence. However, the first observation, hereafter Obs. 1, was obtained just as the system returned to quiescence,  $\sim 10$  days after the peak of an outburst, whereas the second observation, hereafter Obs. 2, occurred  $\sim 135$  days after the prior outburst peak with U Gem well into quiescence, about 60 days before the next outburst would occur. The two observations did not occur after the same outburst but the nature of the outbursts was fairly similar: Both had have fairly "rounded" optical burst profiles peaking at a normal maximum of 8.7-8.8 mag. Neither exhibited a prominent plateau. The outburst preceding Obs. 1 lasted 14.9 days, based on the time above magnitude 13, whereas the outburst before Obs. 2 lasted 14.1 days, and thus both were "wide" outbursts. The two *FUSE* observations were also fairly similar, with planned exposure times of about 13,000 s, as indicated in the observational log presented in Table 1.

The FUSE spectrograph consists of four independent optical channels that combined cover the 905-1187 Å wavelength range (Moos et al. 2000). The optics of two of the four channels are optimized for shorter wavelengths (905-1105Å) with a SiC coating. The optics of the other two channels are coated with LiF and optimized for the longer wavelengths (1000-1187Å). The data are recorded in eight segments, A and B for each of 4 channels, and the eight segments can be combined to cover the full 905-1187 Å range with some overlap. Both observations were taken in the photon-counting time tag mode through the large 30" x 30" (LWRS) aperture. This minimizes slit losses that can occur due to misalignments of the four FUSE channels. Sahnow et al. (2000) describe the FUSE observatory and its in-flight performance in detail.

Although Obs. 1 had been previously reduced by Froning et al. (2001) (denoted "Obs. 4" in that paper), we have re-reduced Obs. 1 and reduced Obs. 2 using the FUSE data reduction pipeline (CALFUSE 2.4.0), and combined the data from the separate channels to produce time-averaged spectra. An important consideration in constructing the time-averaged spectra is that FUSE guides on a single channel, LiF1, and that thermally-induced distortions of the optical benches can lead to significant slit losses in the non-guided channels. To determine whether this problem affected the U Gem data, we constructed spectra in 300 s time intervals and compared the fluxes in the overlap regions of the various channels. Inspection of these data showed that by the end of Obs. 1, U Gem had drifted out of the

apertures of all three non-guided channels. In situations where the flux differences in the overlapping regions is small, we rescaled the data using the strategy described by Froning et al. (2001); if the difference was large, as it was about half of the time for the non-guided channels, we discarded the data. In contrast, during Obs. 2, none of the channels appear to have drifted significantly and all of the data was included in the final combined spectra. In combining the spectra, the channels were weighted according to the errors associated with the individual channel spectra, and regions where the flux calibration is uncertain (i.e. the "worm" on LiF1B at wavelengths > 1150 Å (Sahnow et al. 2000) was excluded).

While not seriously affecting the flux calibration, small thermally-induced motions of the four channels, including the guided LiF1 channel, can also induce small offsets in the wavelength solution. Therefore in the process of combining the data, we also checked for time-dependent errors in the wavelength solution using narrow interstellar (IS) absorption features as fiducials. Specifically, we measured the position of IS O I  $\lambda$ 1039.23 and N I  $\lambda$ 1134.98 by fitting Gaussian profiles to the observed lines. There were no obvious drifts with time in either observation. In Obs. 1, the RMS variation in the measured position of the two lines was 0.01 Å (2 km s<sup>-1</sup>) with a small zero point offset of 6 km s<sup>-1</sup>. In Obs. 2, the interstellar lines were more difficult to measure due to a lower continuum flux level and confusion with a (presumably) photospheric line at 1135 Å. Nevertheless, the RMS variation in line centers was < 0.02 Å (4 km s<sup>-1</sup>), and in this case there was no measurable zeropoint offset.

Since most, if not all, of the FUV light from U Gem arises from the vicinity of the WD and our primary goal is to understand the nature of the emission on the WD photosphere, we removed the smearing effect of the WD orbital motion by shifting the individual 300 s segment spectra to the reference frame of the WD, using the ephemeris of Marsh et al. (1990) and  $K_1 = 107.1 \pm 2.1$  km s<sup>-1</sup> and  $\gamma_1 = 172 \pm 15$  km s<sup>-1</sup> obtained by Long & Gilliland (1999) from a series of high time resolution GHRS spectra of U Gem (Our own analysis of the orbital parameters is discussed in Sec. 3.4). We shifted each 300 s spectrum using these orbital parameters to place all of the spectra at a common velocity, namely the recession velocity of the WD at phase=0, and we combined the shifted spectra to obtain a time-averaged spectrum for each observation.<sup>2</sup> Thus, the time-averaged spectra were corrected for the smearing of the WD spectrum due to its radial velocity motion, while the non-moving interstellar and airglow features were smoothed out in the process. The final time-averaged spectra were rebinned to a wavelength resolution of 0.1 Å and are shown in Fig. 2.

<sup>&</sup>lt;sup>2</sup>Since phase 0 in the ephemeris of Marsh et al. (1990) corresponds to secondary conjunction, and since we shifted the spectra by  $\gamma_1$ , the sum of the gravitational and recessional velocity of the WD, this choice means that photospheric lines from the WD should appear at their rest wavelengths in the shifted spectra.

As anticipated, both spectra resemble that expected from a WD with an atmosphere that contains metals as a result of on-going accretion. In particular, the spectra show absorption from the H Lyman series from Lyman  $\beta$  to the Lyman limit, and a rich set of metal absorption lines. The Obs. 1 spectrum peaks at 1000 Å at  $5.0 \times 10^{-13}$  ergs cm<sup>-2</sup> s<sup>-1</sup> Å<sup>-1</sup>. The Obs. 2 spectrum peaks at 1105 Å at  $2.5 \times 10^{-13}$  ergs cm<sup>-2</sup> s<sup>-1</sup> Å<sup>-1</sup>. The ratio of the Obs. 1 spectrum to the Obs. 2 spectrum is greatest at wavelengths short of 1000 Å (5:1 at 960 Å) and decreases at longer wavelengths (2:1 at 1160 Å), indicating a reddening of the Obs. 2 spectrum and, thus, that the average temperature of the WD is cooler in Obs. 2. The cooling of the WD during quiescence was noted in HUT spectra of U Gem taken 10 (Astro-1; Long et al. 1993) and 185 (Astro-2; Long, et al. 1995) days into quiescence. The shapes of the FUSE Obs. 2 and HUT Astro-2 spectra are nearly identical considered at the 3 Å resolution of HUT. If anything, the FUSE Obs. 2 spectrum is slightly redder, possibly indicating a cooler average WD temperature. The fluxes observed on Astro-2 were slightly greater (10%) than observed with FUSE, also suggesting a cooler average WD temperature at the time of FUSEobservation. Given the calibration uncertainties, however, its also possible that the fluxes were identical in the two mid-quiescence observations. The fluxes from the FUSE Obs. 1 spectrum are about 25% higher than observed with Astro-1 10 days into quiescence.

As shown in Fig. 2, absorption lines of low ionization species of C, N, O, P, S, and Si are observed in both observations. All of the lines seen in Obs. 1 appear in Obs. 2, while there are additional lines of S II and Fe III that appear in Obs. 2 and do not show up in Obs. 1. The lines that appear in both observations generally have larger equivalent widths in Obs. 2. Most of the lines that are seen are from ions that are expected in the metal enriched photosphere of a WD with a temperature of 30,000-40,000 K. The main exception is the O VI  $\lambda\lambda$ 1032, 1038 doublet, which requires a temperature of at least 80,000 K, and therefore must arise along the line of sight to the WD, but not from the photosphere.

A comparison of the individual spectra from Obs. 1 shows very little variability. In particular, the flux measured in the line free region between 1045 and 1055 Å of the Obs. 1 spectrum remains fairly constant throughout the entire integration (with an RMS variability of 2.9%) and no secular trends. However, the continuum fluxes of the 300 s Obs. 2 spectra vary by as much as 25% of the time-averaged Obs. 2 spectrum with an RMS variation of 7.8%. Furthermore, as indicated in Fig. 3, a lightcurve of the Obs. 2 continuum flux plotted against orbital phase shows dips at orbital phase 0.2-0.35 and 0.6-0.85. An Obs. 2 spectrum extracted around the dip between phase 0.6 and 0.85 shows a striking increase in the number and depth of absorption features (see the lower panel in Fig. 3). During the dip, the flux below 970 Å decreases substantially, and nearly all of the lines become much more prominent. The only absorption lines that are not noticeably stronger are those that are already quite saturated, and O VI.

The coverage of Obs. 2 is not complete between orbital phase 0.6-0.85 and the spectra showing the increased absorption come from a single orbit of U Gem; thus, we cannot prove that the absorption at near phase 0.7 is orbitally dependent rather than a secular behavior. However, dips have been seen at similar phases in soft x-ray (Mason et al. 1988), extreme ultraviolet (Long et al. 1996), and FUV (Froning et al. 2001) wavelengths in U Gem in outburst. More importantly, X-ray absorption has been observed in U Gem in quiescence near phase 0.7 by Szkody et al. (1996) and by Szkody et al. (2002) using ASCA and Chandra, respectively. Therefore, phase-dependent absorption is the most plausible interpretation of the time-variable absorption seen in mid-quiescence during Obs. 2 in the FUV with FUSE.

# 3. Analysis

In order to quantify the properties of the WD in U Gem at the time of the two FUSE observations, we have fit the spectra to a grid of synthetic WD model spectra created using Ivan Hubeny's TLUSTY and SYNSPEC codes for calculating the structures and spectra of stellar atmospheres (Hubeny 1988; Hubeny & Lanz 1995). The main model grid covers a range of WD temperatures from 12,000 to 90,000 K, gravities from log g of 8.0 to 9.0, WD rotation velocities ( $v \sin(i)$ ) from 0 (non-rotating) to 500 km s<sup>-1</sup>, and metal abundances from 0.1 to 10 times the solar ratios. The synthetic spectra were computed at fine wavelength resolution ( $\delta\lambda < 0.01$  Å) and convolved with a Gaussian (FWHM = 0.1 Å) to match the wavelength resolution of the FUSE spectra.

Unless otherwise noted, we used a standard least-squares minimization routine to find the models that best approximate the data. We assume that the reddening along the line of sight is negligible, since that is what is expected for the value of  $N_H$  of  $2 \times 10^{19}$  cm<sup>-2</sup>, determined by Froning et al. (2001).<sup>3</sup> For Obs. 2, there is, as described earlier, time-variable absorption. Since this extra absorption is most likely unassociated with the WD photosphere, we first describe fits to the portions of the Obs. 2 data when this extra absorption was not present, and return to the question of the nature of time variability in Section 3.3. Here and elsewhere, when we refer to the unabsorbed spectrum of Obs. 2, we mean the data outside of orbital phases 0.2-0.35 and 0.65-0.85. For Obs. 1, we fit the time averaged spectrum. In fitting the data, we ignored the data near Lyman  $\beta$  airglow emission and around the O VI lines, which are not expected in the photosphere of a WD with a temperature characteristic of U Gem.

 $<sup>^3</sup>$ The reddening has not been measured directly. Verbunt (1987) estimated that it is 0.0 with an upper limit of 0.03 from the absence of a 2200Å feature in IUE spectra.

Based on our past experience with analyzing spectra of WDs in CVs with FUSE, our general approach was to begin with the simplest models, that one might reasonably expect to apply to the data, in this case, models of uniform temperature WDs with approximately solar photospheric abundances. We did not really expect to obtain good fits in a  $\chi^2_{\nu}$  sense both because the systematic errors in the FUSE calibration exceed the statistical errors, and also because the models themselves are subject to uncertainties in, for example, the atomic data. To be confident that a more complicated model really is a better description of the actual physical situation we required not only that  $\chi^2_{\nu}$  improve, but also that one can point to specific regions or characteristics of the spectrum where the more complicated model provides a qualitative improvement in the data. This reflects our bias that others have sometimes relied too much on improvements in  $\chi^2_{\nu}$  alone to assert a real physical improvement our understanding of spectrum.

# 3.1. Uniform temperature WD model fits

#### 3.1.1. Solar abundance models

We first attempted fits assuming the surface temperature of the WD was uniform during both observations. As a fiducial for further fits, we first fit the spectra to models with solar abundances. Given that we fixed  $N_H$ , E(B-V) and  $\log g$ , the variables for the fiducial fits were the temperature  $T_{WD}$  of the WD,  $v \sin (i)$  of the WD, and N, an overall normalization. For a WD at a distance D, the radius  $R_{WD}$  is given by  $D \sqrt{N/4\pi}$ .

For Obs. 1, as indicated in Table 2, the best fit log g=8.5 model has a temperature  $T_{WD}$  of 43,600 K, and a  $v \sin(i)$  of 152 km s<sup>-1</sup>. Assuming that the WD is not obscured, the model normalization combined with the known distance of 100.4±3.7 pc (Harrison et al. 2004) implies the radius of the WD,  $R_{WD} = 5.0 \pm 0.2 \times 10^8$  cm, where here the errors are those associated with the distance uncertainty. The model, as is shown in Fig. 4, provides a reasonable qualitative, if not statistical ( $\chi^2_{\nu} = 6.7$ ), fit to the data. The model recreates the shape of the continuum at wavelengths longer than 970 Å including the Lyman  $\beta$  and Lyman  $\gamma$  line profiles. Many of the absorption lines in the spectrum also have approximately the correct widths and depths. The most noticeable failure of the model to match the observed flux is at wavelengths short of 970 Å where there is excess flux not predicted by the model.<sup>4</sup> The biggest problems with features in the spectrum are near 990 Å, where the

 $<sup>^4{</sup>m T}_{WD}$  is somewhat sensitive to the reddening. Setting E(B-V) to 0.03 results in a best fit with  ${
m T}_{WD}$  of 46,400 K and  $\chi^2_{
u}$  of 6.2; setting it to 0.06 results in 49,700 K and  $\chi^2_{
u}$  of 5.9. However, the problem of excess flux in the observed spectrum shortward of 970 Å remains. The improvement in  $\chi^2_{
u}$  with reddening has to

observed N III, He II and S III feature is mush stronger in the data than in the models, and near the Lyman  $\beta$  and O VI complex. As noted earlier, a pure WD model was not expected to account for O VI, however the excess emission around Lyman  $\beta$  was not necessarily expected. One likely possibility is that the excess is due to emission from the disk.

Similar quality fits to the Obs. 1 spectrum can be also be obtained with  $\log g = 8$  and  $\log g = 9$  models. As enumerated in Table 2, the best fitting  $\log g = 8$  model has  $T_{WD}$  of  $40,700 \text{ K}, v \sin(i) \text{ of } 163 \text{ km s}^{-1}, R_{WD} \text{ of } 5.3 \times 10^8 \text{ cm}, \text{ and } \chi^2_{\nu} \text{ of } 7.2.$  This temperature is, as one might expect, very similar to the value of 43,410 K, obtained by Froning et al. (2001) using the same gravity and solar abundances. The differences most likely arise from small changes in the FUSE calibration and possibly a different selection of the exact wavelengths to fit. For log g =9, the best fit model has  $T_{WD}$  of 47,100 K,  $v \sin{(i)}$  of 135 km s<sup>-1</sup>,  $R_{WD}$ of 4.8, and  $\chi^2_{\nu}$  of 6.5. While all of the model fits are unacceptable in a statistical sense, it is interesting that the fits seem to favor higher gravities. Higher gravity models would be expected to provide a better fit, given estimates of the mass of the WD in U Gem. The main reason that higher gravity models fit the data better is that they provide a somewhat better fit to the region of the spectrum near the Lyman limit; other differences in a qualitative sense are quite minor. The difference in temperature that results from the various gravities is primarily due to changes in the profile of the Lyman lines. The Lyman lines become more prominent as the gravity increases and less prominent as the temperature increases. Since the spectrum one is fitting does not change, using higher gravity models results in a higher temperature (and a correspondingly smaller radius) for the WD in a system.

For Obs. 2, the results of a similar fit to the unabsorbed portion of the data using solar abundance models is illustrated in Fig. 5. The best-fit log g=8.5 solar-abundance model, shown as the solid red line, has  $T_{WD}$  of 30,300 K,  $v \sin(i)$  of 90 km s<sup>-1</sup>,  $R_{WD}$  of  $3.4 \times 10^8$  cm, and  $\chi^2_{\nu}$  of 6.8. Qualitatively, the successes and the failures of the model fit to the Obs. 2 spectrum are rather similar to that of Obs. 1. The model reproduces the shape of the continuum at wavelengths > 970 Å and the wings of Lyman  $\beta$ , but underestimates the flux at wavelengths less than 970 Å. The line cores of Lyman lines (Lyman  $\beta$  through Lyman  $\delta$ ) are not well fit. All show similar profiles of excess emission that could come from double-peaked emission from the disk. GHRS spectra of U Gem during quiescence show evidence for double-peaked disk emission in the core of Lyman  $\alpha$  (Long & Gilliland 1999). Nearly all of the metal lines present in the spectrum exist in the model, with the exception of S VI  $\lambda\lambda$ 933.4, 944.5 and O VI  $\lambda\lambda$ 1031.9, 1037.6 (the model line close to O VI  $\lambda$  1037.6 is C II  $\lambda$ 1037.0). In contrast to the situation, in Obs. 1 however, it is clear the lines in the

do with the fact that higher reddening allows a better fit to the continuum longward of 1050~Å

spectrum are deeper than those in the model. The biggest problems are with the strong absorption features near 990Å(which was a problem with the Obs. 1 spectrum as well) and near 1085 Å. The feature near 1085 Å is primarily due by a N III triplet, as the HeII  $\lambda$ 1085 line is much less weaker than at the higher temperatures of the WD in Obs. 1.

# 3.1.2. Single temperature models with scaled solar metallicities

We next considered the possibility that the photospheric abundance ratios were approximately solar, but that the overall metallicity of the photosphere was either sub- or super-solar.

For Obs. 1, allowing the metallicity to vary does not significantly improve the fits, either in a qualitative or quantitative sense. The best fits all have a metallicity of  $\sim 1.4$  times solar, but the WD temperatures, radius and rotational velocities are almost identical to those obtained when the metal abundances were solar. Furthermore the difference in  $\chi^2_{\nu}$ , as a comparison of Tables 2 and 3 shows, is very small.

By contrast, for Obs. 2, allowing the metallicity to vary reduces the value of  $\chi^2_{\nu}$  for log g = 8.5 models from 6.8 in the solar case to 6.0 for the best fit which has a metallicity that is 3.9 times solar. This model reproduces the strengths of S III  $\lambda$ 1077.1, S IV  $\lambda\lambda$ 1062.7, 1073.0, Si III  $\lambda\lambda$ 993.5, 1108.4, 1110.0, 1113.2, and Si IV  $\lambda\lambda$ 1122.5, 1128.3 better, and this allows a better fit to the level of the continuum as well. As was the case for Obs. 1, there is a discrepancy in the fits to the Si III line complexes. Fitting the Si III lines around 1110 Å require abundances that produce lines that are too strong at 1140 Å and 1155 Å. There is evidence for a lower C abundance and enhanced N abundance based on the fit with scaled abundances: The C II lines  $\lambda$  1010.3, and C III  $\lambda$ 1175.3 are all too strong in the scaled abundance model, and NI 1134.2, N II  $\lambda$ 1085.3, and N III  $\lambda$ 989.8 are too weak.

Based on the fits to the data there is a suggestion that the average metallicity is higher in mid-quiescence (z = 3.3-4.7) than immediately after outburst (z = 1.3-1.5). Whether this is a real physical effect is unclear. What is clear however is that there are some elements, especially N, that have lines that are significantly deeper than expected from our scaled-metallicity grid, and other elements, especially C, that have lines that are weaker than predicted from the best fits obtained from the scaled-metallicity model grid. There is no real reason to expect that all of the metal abundances in U Gem should scale with solar ratios, and indeed recent analyses of HST spectra of U Gem suggest evidence for CNO processing in the form of low C and high N abundances (Sion et al. 1998; Long & Gilliland 1999). While the 1150-1710 Å spectral range of the HST spectra contains a number of well-observed C

lines, it contains only one prominent N transition, N II  $\lambda 1169.86$ , and this is in a portion of the spectrum where the HST spectrographs tend to be less sensitive. The FUSE wavelength range contains a different set of lines, and in particular a number of prominent N lines. Froning et al. (2001), in discussing the spectrum of Obs. 1, noted that the strengths of the N and C lines did indicate that the N lines were strong relative to solar, while the C lines appeared weaker.

# 3.1.3. Abundances of individual elements

To extend the results of the scaled metallicity modeling, we then attempted to constrain the abundances of the elements, N, C, Si, and S, that are responsible for most of the metal features in the spectra. We first constructed four grids of log g = 8.5 model spectra in which the abundances of all elements except one, either C, N, Si, or S, were fixed at their solar values. The fitted variables in these models therefore were  $T_{WD}$ ,  $v \sin(i)$  and the abundance of either N, C, S, or Si. Finally, we created small grids of models with fixed  $T_{WD}$ , in which all N, C, Si, and S, were varied simultaneously. The purpose of the first part of this procedure was determine which elements had the dominant effect on the fits. The purpose of the second part was to account for the effects of having several transitions of different elements contributing to a single feature in the spectrum.

In Obs. 1, the improvement in  $\chi^2_{\nu}$  in the single element fits were most dramatic for N. In particular, for log g=8.5, changing only the N abundance to 33 times solar reduced  $\chi^2_{\nu}$  to 5.4 compared to 6.7 for a solar or scaled abundance model. The higher N abundance provides a much better fit to N III  $\lambda$ 990, though N III  $\lambda$ 1002, 1003, and 1006, which were too strong in the solar model, are even more discrepant in the supersolar model. Varying C alone resulted in a best fit abundance ratio of 0.2, and reduces  $\chi^2_{\nu}$  to 6.5. The subsolar C abundance improves the fits to the profile of C III  $\lambda$  1175 and to the strengths of the weak C III  $\lambda$ 1125 and C IV  $\lambda$ 1169 lines. Allowing the S abundance to rise to seven times solar also reduced  $\chi^2_{\nu}$  to 6.5; this improved the fits to S IV  $\lambda\lambda$ 1063, 1173. For Si, the best fit abundance ratio was 0.8 times solar, and  $\chi^2_{\nu}$  was 6.7, the same as for the scaled abundance fit. One problem with Si is that the Si III  $\lambda$  1110 complex is too weak in the model even though the Si IV  $\lambda\lambda$ 1122,1128 doublet is well fit.

For Obs. 2, like Obs. 1 varying the abundances of N produced a significant reduction in  $\chi^2_{\nu}$  compared to fits with solar abundance models. Specifically, beginning with a solar model, and varying N, resulted in a best-fit N abundance that was 30 times solar, and  $\chi^2_{\nu}$  of 6.2, and clear improvement over the value of  $\chi^2_{\nu}$  of 6.8 for pure solar abundance models. As for Obs. 1, the main improvement was near N III  $\lambda$ 990. Fitting a C abundance of 0.2 solar

decreases the  $\chi^2_{\nu}$  of the fit to 6.5, and the model provides a much better fit to C II  $\lambda$ 1010.3 and C III  $\lambda$ 1175.3. As was the case for Obs. 1, the best fit for S abundance was high, of order 4 times solar, but the improvement in  $\chi^2_{\nu}$  to 6.7 was modest, indicating that the spectrum is not very sensitive to the S abundance. Unlike Obs. 1, changing the Si abundance had a large effect. Specifically, the model with a and abundance of 4.7 times solar resulted in a  $\chi^2_{\nu}$  of 5.8. which was not only considerably lower than for the solar case, but also less than the value 6.0 obtained the scaled abundance models. At a temperature of about 30,000 K, Si II also contributes to the formation of the feature at 990 Å.

The best fits for uniform temperature WD models were obtained when all of the abundances of all of the elements were allowed to vary independently. For Obs. 1, when a log g=8.5 30,000 K models were generated, the best fits were obtained when C, N, Si, and S, had abundances of 0.35, 41, 1.4, and 10 times solar; for Obs. 2, using log g=8.5 43,000 models, the best fits yielded surprising similar abundance values of 0.30, 35 4, and 6.6 times solar. The best fit values of v sin v were 150 and 250 km s<sup>-1</sup> for Obs. 1 and 2, respectively. The value of v is a shallow function of v sin v values of 50 km s<sup>-1</sup> lower or higher produce have values of v that are only larger by less than 1%. Although general trends in relative abundances remain the same, there is a positive correlation of overall metallicity with v sin v sin v in the models with scaled metallicities. The best fits are shown as the black lines in Figures 4 and 5 for Obs. 1 and 2. The improvements in the model fits are generally localized to the lines, as one would expect, and the overall improvement in v is quite significant, but not enough to provide a good statistical fit to the data.

Our basic conclusions with regard to abundances are that the FUSE spectra do provide strong support for CNO processing of material in U Gem, consistent with previous modeling efforts (Sion et al. 1998; Long & Gilliland 1999; Froning et al. 2001), and a strong suggestion of Si overabundance. The spectra also hint at S overabundance as well, and the apparent overabundance is large, but the identifiable affects on the spectra are small, and hence we feel this result to be fairly uncertain. As shown in Figures 4 and 5, it is also important to point out that there are examples where some transitions of the an ion are well modeled, but others are not, suggesting either additional components to the absorption, or limitations in the synthetic spectra.

Regardless of which set of abundances are utilized in fitting the FUSE spectra of U Gem, the uniform temperature model fits to the Obs. 1 and Obs. 2. spectra indicate that the WD has cooled by 12,000 - 16,000 K from the end of the outburst to mid-quiescence, depending on the value assumed for log g. This drop in temperature is greater than the more typical value of 8,000 K that has been reported previously analyses with other UV

spectrographs, e.g. *HST* (Long et al. 1994), and HUT (Long, et al. 1995). The apparent radius of the WD is about 15% larger in Obs. 2 than Obs. 1; this result is consistent with the previous studies, and was in fact first seen with *IUE* (Kiplinger et al. 1991); it is one of several reasons for considering more complicated models for the UV spectra of U Gem, especially in the immediate post-outburst period.

# 3.2. Two-component WD fits

As noted above, uniform T modeling of the spectrum of U Gem just after outburst and far from outburst suggest a larger radius for the WD far from outburst than at outburst. This is essentially a restatement of fact originally commented on by Kiplinger et al. (1991) that the WD flux is falling more slowly than suggested by the apparent change in the temperature of the WD, and which led Long et al. (1993) to suggest that a hot accretion belt might exist on the WD.

Using the HUT, Long et al. (1993,1995) found that single-temperature WD models underestimated U Gem's UV flux below 970 Å, similar to the failure of the WD models described in Section 3.1 to accurately predict the flux at the short wavelength end of the FUSE spectra. The discrepancy in the HUT analysis was mitigated by adding a second high temperature WD component to the model that covered 15% of the WD surface close to outburst and 1% of the surface far from outburst.

Consequently, we carried out fits of to the data from Obs. 1 and 2 assuming two separate regions on the WD surface. We allowed different metallicities and different rotational velocities in each region of the white dwarf surface and carried out fits for log g=8.0, 8.5, and 9.0. The results are summarized in Table 4. The results for log g=8.5 are typical. In this case, allowing two WD components in the fit to the Obs. 1 spectrum, we find a cool component with  $T_{WD}=28,500$  K that covers 82% of the WD surface and a hot component with  $T_{WD}=70,000$  K that covers 18%. The cool and hot model components have scaled abundances of 1.5 and 8.9 times solar and WD rotation rates of 87 and 243 km s<sup>-1</sup>, respectively.  $\chi^2_{\nu}$  improves to 5.7 from 6.2 in the corresponding single component model. The improvement in  $\chi^2_{\nu}$  is primarily due to an improvement in the fit at the shortest wavelengths. The higher temperature component dominates the flux throughout, as indicated in Fig. 6, but especially at the shortest wavelengths. A WD photosphere with a temperature of 60,000 to 70,000 K has fewer lines than one with lower temperature and so the two temperature fits generally favor a more metal enriched atmosphere than one with solar abundances. The lines are fairly well fit with the two-T model, although N III 989 and C III 977 remain a problem. In this particular fit, the rotational velocity of the higher temperature components is somewhat higher, 243 km s<sup>-1</sup>, than the lower temperature component, 87 km s<sup>-1</sup> as expected if the hot component is rapidly rotating. But this is clearly not a robust result, since the log g = 9 fit of the same type has the cooler component rotating more rapidly.

A two component fit to the Obs. 2 spectrum, using the log g=8.5 model grid also yields a modest improvement  $\chi^2_{\nu}$ , 5.7 compared to 6.0 for the case of a single component with variable abundances. The lower temperature component has  $T_{WD}$ =26,100 K, and an abundance that is 5.7 times solar. It covers 81% of the WD surface, very similar to the percentage covered by the cool component in Obs. 1. The higher temperature component has a temperature of 34,500 K. The total normalization for the WD with this fit is  $5.7 \times 10^{-23}$ , which corresponds to a radius of  $6.6 \times 10^8$  cm, compared to  $5.5 \times 10^{-23}$  and  $6.5 \times 10^8$  cm for a similar fit to the Obs. 1 spectrum. In the case of the best fit model for log g=8.5, the two temperature fit seems to resolve the problem with a WD that grows in radius during quiescence. A comparison of the fits obtained for log g = 8 and log g = 9 yields a similar results. Thus, the 2-T WD model fits to the FUSE data do seem to provide some modest support for the idea that there is a heated region on the surface of the WD.

The argument that a second source in the spectrum of U Gem arises from the WD surface would be stronger if it could be shown that a competing model gave a less significant result. One alternative would be residual disk emission, but unfortunately our understanding of how to model an accretion disk in or near quiescence is very primitive. Therefore, we opted to see whether a simple power law model for the second component would produce a better or worse fit to the data. The variables for this fit were  $T_{WD}$ , z,  $v \sin(i)$ , and the normalization of the WD, plus a power law index and normalization for the second component. The best fits for Obs. 1 and 2, assuming log g=8.5 for the WD had  $\chi^2_{\nu}$  of 5.5 and 5.6 respectively, just slightly worse than for the 2-T WD model fits. The implied WD temperatures were similar, 41,000 K and 29,200 K, to those obtained for the single T WD models. Qualitatively, as shown in Fig. 7, the model fits looked rather similar to those obtained for the 2-T WD model fits.

On the basis of this analysis, we conclude that while there are real departures in the shape of the spectrum from a simple LTE WD model in U Gem immediately after an outburst, a physical interpretation in terms of two-temperatures on the WD surface is not demanded by the data. We will return to the nature of the second component in Sec. 4.1.

# 3.3. Phase-dependent absorption

The phase-resolved spectra of Obs. 2 show clear evidence of variable line absorption. As illustrated in Fig. 8, the same lines contribute to the absorption during all phase intervals. Furthermore, many of the same lines appear in the portions of the phase-resolved spectra we have designated as "unabsorbed". The phase 0.6-0.85 absorption is very similar to that between phase intervals 0.2-0.35, except that the lines are deeper in the phase 0.6-0.85 spectrum. The lines are not exactly at zero velocity with respect to the WD. At phase 0.2-0.35, the lines are blue-shifted (in the frame of the WD) by  $\sim 50 \,\mathrm{km \ s^{-1}}$  while at phase 0.6-0.85 the lines are red-shifted by  $\sim 120 \,\mathrm{km \ s^{-1}}$ . These wavelength shifts are important since they imply that the absorption is not the result of changes in the photosphere itself.

In an attempt to characterize the absorption, we have modeled the Obs. 2 spectra in terms of a WD photosphere and a "slab" or veil of overlying material. For simplicity, we have assumed solar abundances and LTE conditions in the slab material. Neither of these conditions is likely to be correct in detail, but alternatives are all more complicated and without some physical model seem unjustified at this time. Each slab is described by its density, temperature, turbulent velocity and column density. Our procedure for modeling the absorption of the slab is as follows. Using an option of Ivan Hubeny's SYNSPEC program, we first calculate opacities as a function of wavelength in the slab as a function of density and temperature. To account for the effects of turbulence, we then smooth the opacities, and calculate the transmission of the slab as a function of wavelength. We also shifted the spectra by either -0.18 or 0.44 Å, to account for the offset of the absorption lines in the observed spectra. We created a grid of models for temperatures from 5,000 to 25,000 K, for densities  $(N_H = N_{HI} + N_{HII})$  ranging from  $10^9$  cm<sup>-3</sup> to  $10^{13}$  cm<sup>-3</sup>, for turbulent velocities  $v_{turb}$  ranging 0 to 300 km s<sup>-1</sup>, and for column densities ranging from log N<sub>H</sub> of 18 to 23. In attempting to fit the data, we assumed that the underlying continuum was generated from the WD photosphere and that the photosphere had solar abundances.

In attempting to the fit the data, we initially used a standard  $\chi^2_{\nu}$  minimization technique and fit the same portions of the data that we had used in the previous fits. However, this resulted in fits that fell well below the observed spectrum where there is little or no absorption, especially in the phase 0.6-0.85 spectrum. The reason this occurs is that a standard  $\chi^2_{\nu}$  fit heavily weights the points with the smallest errors, which are the data points with greatest absorption, dragging the model continuum down in instances where the model is unable to reproduce all of the absorption lines. Therefore we opted for an approach that we believe gives a better "eye-ball" description of the data at the expense of formal statistical correctness. Specifically, we have adopted a two-pass approach to fitting the data, which consists of using an initial standard  $\chi^2_{\nu}$  minimization fit to screen out highly discrepant

points, namely points with an initial  $\chi^2_{\nu}$  of 25 or greater. We then refit the remaining data points (about 95% of those considered in the initial fit) to the models to find a fit that describes most of the data points. This results in fits that follow the shape of the continuum well and approximates most, but not all, of the lines. There are a number of other ways that can be used to obtain fits that qualitatively represent the data including limiting the contribution to total  $\chi^2_{\nu}$  rather than eliminating discrepant points, or using an asymmetric metric that gives extra weight to data points where the model underestimates the data. These techniques produce similar results qualitatively, although they tend to yield best fits with somewhat larger line widths, expressed as turbulent velocities, in the fits described below. Our impression is that the lines widths using our preferred technique are a more accurate representation of the data.

We applied this technique to each of the Obs. 2 spectra, the "unabsorbed" spectrum, the phase 0.20-0.35 spectrum, and the phase 0.60-0.85 spectrum. Results of the fits assuming normal abundance log g =  $8.5~\mathrm{WD}$  atmospheres and slabs with densities of  $10^{13}~\mathrm{cm}^{-3}$  are shown in Fig. 9 and tabulated in Table 5. The WD temperatures, 30,500 K for the "unabsorbed spectrum", 29,400 K for the phase 0.20-0.35 spectrum, and 29,900 K for the phase 0.6-0.85 spectrum are close to the value of 29,700 K derived for a simple uniform temperature WD model with variable abundances. For densities of  $10^{13}$  cm<sup>-3</sup>, the effective temperature of the veil was about 10,000-11,000 K for both the phase 0.2-0.35 and the phase 0.6-0.85 spectrum. As expected, the column density of ionized and unionized hydrogen was higher in the fit to the phase 0.6-0.85 spectrum (log  $N_H = 21.3$ ) than in the phase 0.20-0.35 spectrum (20.7). To first order the properties of the slab are the same during both periods when absorption is observed. Similar results, both in terms of the qualitative nature of the fits and in terms of the column densities are obtained when other slab densities are considered. Specifically, the derived WD temperatures are similar and the column densities derived for the slab are similar. However, the temperature derived from the plasma is somewhat higher, 12,000-13000 K for a density of  $10^9 \text{ cm}^{-3}$ , instead of 10,000-11,000 K. The higher temperature that is required with lower densities is a direct consequence of the simplifying assumption that the gas is in LTE.

A disturbing possibility that must be considered is that the absorption is not confined to phase 0.2-0.35 and 0.6-0.85. This is hard to rule out completely, but Fig. 9 does provide a certain amount of comfort. The effects of the slab on the "unabsorbed" spectrum are relatively minor compared to those seen in the fits to the phase 0.20-0.35 and 0.60-0.85 spectra.

# **3.4.** Orbital parameters from the *FUSE* data

The orbital parameters of the WD in U Gem have been measured several times. The most detailed study was carried out by Long & Gilliland (1999), who used the GHRS to obtain a series of time-resolved GHRS spectra covering the wavelength range 1168-1448 Å to derive a value of  $K_1$  of  $107 \pm 2.1$  km s<sup>-1</sup>. Long & Gilliland (1999) found that low ionizationstate lines of C II, Si II, and Si III had an average  $\gamma$  velocity of 172.1 $\pm$ 15 km s<sup>-1</sup>, whereas the higher ionization-state lines of Si IV and N V had lower values of  $124\pm15~{\rm km~s^{-1}}$  and  $102\pm10$ km s<sup>-1</sup>, respectively. Since the low ionization stale lines are expected in the photosphere of a 30,000 K WD, they concluded that these lines provided a good measurement of  $\gamma_1$ , that is the velocity shift due both to the recessional velocity of the U Gem system and the gravitational redshift of the WD surface. They suggested that the higher ionization state lines were formed at a location above the WD surface. N V is not expected in a WD photosphere with  $T_{WD}$ of 30,000-40,000 K, and the Si IV lines were stronger than predicted for the Si abundance derived from Si II and Si III. The results of their study were in agreement with the result reported slightly earlier by Sion et al. (1998) based on observations of the Si III multiplet at 1300 Å at two specific phases in the orbital period; Sion et al. found  $K_1$  and  $\gamma_1$  to be 107 km s<sup>-1</sup> and 161 km s<sup>-1</sup>, respectively, but gave no error estimates. As previously noted, we used this  $K_1$  velocity to produce the average spectra for spectral analysis.

In principle, the FUSE observations described here provide an independent measurement of  $K_1$ , since they have good phase coverage and since FUSE has more than sufficient resolution to measure velocities in this range, and so we attempted such an analysis. Here, we used unshifted 300 second spectra.<sup>5</sup>. We restricted our analysis to data obtained with the LiF1 channel since this was the channel used for guiding. We rebinned the original data to 0.1 Å to improve the S/N somewhat. We measured the central wavelengths of several of the strongest absorption lines in each of the individual time-resolved spectra from Obs. 1 and Obs. 2. For this we used the IRAF SPECFIT task described by Kriss (1994). We fit the lines in SPECFIT using Gaussian line profiles and taking into account the errors in the rebinned spectra. For Obs. 1, we fit the Si IV  $\lambda$ 1122 Å and Si IV + P V  $\lambda$ 1128 Å transitions. For Obs. 2, we fit these transitions and added the Si III  $\lambda$ 1110 and 1113 Å lines (we also fit the 1108 line but the fits were poor due to low S/N and were not used). We compared the central wavelengths of each line to the wavelength center in the time-averaged LiF1 spectrum for each observation.

We then converted the wavelength shifts to velocities and fit a sine function with the appropriate period to all the lines in an observation to determine the radial velocity amplitude

<sup>&</sup>lt;sup>5</sup>For this portion of the analysis, we used spectra created with CALFUSE 3.1.

 $K_1$ . We allowed the amplitude and phase of the sine curve to vary, but not the period (or eccentricity). After the initial fit, we created a time-averaged spectrum with the orbital motion removed, recalculated the central wavelengths of each line, found new velocity shifts for the lines and refit the wavelength shifts. This cycle was repeated several times until the fits central wavelengths in the time-averaged spectra were stable.<sup>6</sup> Figure 10 shows the best fits for Obs. 1 and Obs. 2. The uncertainty on the amplitude represents the range of amplitudes that yielded fits within  $\chi^2+4.61$  of the best fit to establish 90%, or 1.6  $\sigma$ , confidence limits (Lampton et al. 1976). Finally, for Obs. 2, we repeated the fits using only the unabsorbed phases: 0 - 0.2, 0.35 - 0.6, and 0.85 - 1.

For Obs. 1, the best fit sine curve has an amplitude  $K_1$  of  $122\pm10$  km s<sup>-1</sup> and a phase offset from the ephemeris of Marsh et al. (1990) of  $0.04\pm0.01$ . The fit had  $\chi^2_{\nu}=1.2$ . For Obs. 2, the best fit sine curve has a larger amplitude of  $132\pm6$  km s<sup>-1</sup> and a phase offset from the ephemeris of  $-0.04\pm0.01$ , with  $\chi^2_{\nu}=2.4$ , but this is most likely affected by the effects of the additional absorption discussed in Section 3.3. If the fit is restricted to data from "unabsorbed" phases, then the amplitude drops to  $117^{+9}_{-8}$  km s<sup>-1</sup>, which is close to that obtained for Obs. 1, even though  $\chi^2_{\nu}$  remains quite high at 2.3. The quality of the fits is shown in Fig. 10. Alternative approaches to obtaining  $K_1$ , such as simple cross-correlation measurements gave very similar results. Thus the FUSE data suggest a slightly higher value of  $K_1$  than the two HST-based studies. However, the errors on the FUSE  $K_1$  velocities are fairly large (as a result of the fact that FUSE is a much smaller telescope than HST), and the HST and FUSE values differ formally at less than  $2\sigma$ .

Next, we attempted to calculate absolute wavelengths for lines by measuring their central wavelengths in a time-averaged spectrum with the orbital motion removed, using the amplitudes calculated above. First, we determined corrections to the absolute wavelength solution by measuring the central wavelengths of several interstellar lines (O I  $\lambda$ 1039 Å, Ar I  $\lambda$ 1048 Å, and the N I  $\lambda$ 1134 Å triplet) in the original time-averaged spectrum. The absolute wavelength offset corrections were small: 4 km s<sup>-1</sup> for Obs. 1 and 8.5 km s<sup>-1</sup> for Obs. 2. These offsets are very similar to the values we had obtained in our original reduction of the data with CALFUSE 2.4, discussed in Sec. 2 . (Note that the reduced FUSE spectra are already corrected for a heliocentric motion as part of the calibration pipeline). We then measured the central wavelengths in the U Gem lines in the orbital motion-corrected spectrum

<sup>&</sup>lt;sup>6</sup>One could have alternatively fit the line centers to a amplitude, a phase, and a velocity offset. This technique avoids the iterative process that we describe here, and indeed yields similar results for  $K_1$ . However, the technique we used yielded better  $\chi^2_{\nu}$  than a non-iterative fit to a single amplitude, offset, and phase for all of the lines, presumably due to the fact that the measurements of the line centroids of the average spectrum were measured more consistently as a result of our iterative approach.

and compared them to their laboratory values. To focus on WD motion rather than that of any intervening material, we used only the non-absorbed spectra and adopted 118 km s<sup>-1</sup> as the  $K_1$  amplitude in Obs. 2.

We measured S IV  $\lambda 1062$  Å, S IV  $\lambda 1073$  Å, Si IV  $\lambda 1066$  Å, Si III  $\lambda 1110$  Å, Si III  $\lambda 1110$  Å, Si III  $\lambda 1113$  Å, and Si IV $\lambda 1122$  Å for both observations. We omitted the  $\lambda 1128$  Å transition because it is a blend of Si IV and P V. We initially measured the wavelengths of each transition assuming Gaussian profiles for each of the lines. All of the transitions did show positive  $\gamma$  velocities measured in this manner. However, the  $\gamma$  velocities range from about 65 km s<sup>-1</sup> for S V  $\lambda 1062$  to a maximum of 155 km s<sup>-1</sup> for the Si III  $\lambda 1108$ . And it was immediately clear that this approach led to significant inconsistencies in the  $\gamma$  velocities of individual components of the same multiplet, especially Si III. Several of the lines are obviously asymmetric, and this clearly explains why for example, the shift for S IV  $\lambda 1062$  Å, when measured form a Gaussian fit to that feature, was less than the other two members of that multiplet in Obs. 1, probably as a result of a contribution to this line from another line. And in Obs. 2, its clear that one is affected by the effects of absorption as the lines are broader and sometimes appear to have multiple minima.

Therefore, in the end, we elected to measure the minimum flux value of each of the transitions. Results of these measurements are shown in Table 6 and the portions of the spectra that were measured are shown in Fig. 11. For Obs. 1, the average value of  $\gamma$  is 144.9 km s<sup>-1</sup> and the standard deviation from the mean is 13.9 km s<sup>-1</sup>; for Obs. 2, the average is 131.2 km s<sup>-1</sup> and the standard deviation is 10.2 km s<sup>-1</sup>. These values are close to the values of  $\gamma$  reported by Long & Gilliland (1999) and by Sion et al. (1998) using GHRS, but they do not show the pronounced change in  $\gamma$  velocity with ionization state reported by them. None of the ionization lines have  $\gamma$  velocities as great as measured by them for Si III, which they argue corresponds to  $\gamma_1$  of the WD photosphere. As was the case for the measurement of K<sub>1</sub>, the difference is however significant at most at the 2  $\sigma$  level.

A possible way to bring the measurements into closer agreement would be to question the absolute wavelength scale. The FUSE observations were made through the LWRS aperture, and so in principle, the absolute wavelength scale can be in error by as much as 0.25 A, or about 65 km s<sup>-1</sup>. However, the typical error is thought to be less than this. Bowen (2005, as quoted on the FUSE website) has compared velocities of  $H_2$  lines measured with FUSE to interstellar Cl I  $\lambda$ 1347 and finds a mean error of  $\pm$ 10±6 km s<sup>-1</sup>. We have attempted to compensate for offsets in the wavelength scale by referencing our wavelength scale to those of IS lines. Nevertheless, this could be a problem. Long & Gilliland (1999) note that the core of  $\pm$ 10±6 km s<sup>-1</sup>. The core of  $\pm$ 10±6 km s<sup>-1</sup>.

are the same, we would need to add 30 km s<sup>-1</sup> to our velocities to put them on the GHRS wavelength scale. If that is the case, then our mean  $\gamma$  velocities would be much closer to those derived with GHRS for low ionization state lines.

In view of these uncertainties, our conclusion is that the orbital parameters derived from the analysis of the FUSE data are not to be preferred to HST values, even though they do suggest that if a capability for high resolution UV spectroscopy is restored to HST, that it would be desirable to remeasure especially the  $\gamma$  velocity of the WD. As will be discussed in Section 4.4, there is currently a discrepancy between the radius of the WD derived from the normalization of the spectrum and the radius implied by the gravitational redshift, and the latter requires an accurate measure of  $\gamma_1$ .

#### 4. Discussion

# 4.1. WD Cooling

The FUSE observations confirm once again (Kiplinger et al. 1991; Long et al. 1993, 1994) that the WD in U Gem cools, or appears to cool, between outbursts. The cooling is apparent in the decline in FUV flux, the fact that the flux at short wavelengths declines more than at long wavelengths and the fact that Lyman  $\beta$  is broader far from outburst. The average cycle time for outbursts of U Gem is 132 days (Ak et al. 2002). The only detailed study of a single interoutburst interval was conducted with IUE (Kiplinger et al. 1991) and that study appears to show that the (1620 Å) UV flux declines slowly (with some scatter) throughout the entire interval. Unless STIS is recommissioned or COS installed on HST on an upcoming Shuttle mission, it seems unlikely that this situation will change. This is unfortunate since it makes separating the physical process that contribute to the flux decline difficult.

Cooling of the WD is observed in other systems. The best examples of this are probably, VW Hyi and WZ Sge. In VW Hyi, the WD is heated to either 23,000 K in a normal outburst or 27,000 K in a superoutburst. It then cools back 19,000 K with an exponential decay time constant of 2.8 or 9.8 days for a normal or superoutburst, respectively (Gänsicke & Beuermann 1996). The differences in the two situations are presumably associated with the fact that superoutbursts deposit more and more matter on the WD, and last longer than normal outbursts. In this regard, typical outbursts of U Gem including the outburst that preceded Obs. 1 are more like superoutbursts of VW Hyi in terms of integrated energy and duration. Since typical outbursts in VW Hyi are separated by 28 days (Ak et al. 2002), we cannot follow long term cooling trends in VW Hyi. WZ Sge represents the opposite extreme.

It went into outburst in 2001, the first time in 22 years. The WD was heated to 26,000 K (at least), and has in the past 4 years cooled with a time constant of about 180 days to 15,000 K (Long et al. 2004; Godon, et al. 2006), close to its pre-outburst temperature of 14,800 K (Cheng et al. 1997). The WZ Sge outburst lasted about 24 days (followed by a series of echo outbursts); this and the very long interoutburst period presumably account for the long decay time constant.

A variety of processes are likely to contribute to the heating and cooling of the WD, and disentangling these processes is one of the main challenges of CV research today. The mechanism that seems most likely to dominate on long time scales (and a process that allows the creation of detailed models) is compression heating; this is the physical response of the WD to the deposition of additional mass on the WD surface (Sion 1995; Townsley & Bildsten 2002; Godon & Sion 2002; Piro et al. 2005). The WD is hotter than before, due both to the release of gravitational energy as the star rearranges its internal structure and to slow burning of material at the base of the accreted envelope. Sion (1995) showed in particular that the basic properties of the WD in U Gem, heating by of order 10,000 K and cooling that had timescales of months, could be produced for plausible accretion scenarios. Other processes that could also be involved include direct heating of the outer atmosphere of the WD during the outburst (Pringle 1988) and elevated accretion just after an outburst, perhaps associated with a coronal flow (Meyer & Meyer-Hofmeister 1994). Direct heating during the outburst affects the outermost layers of a WD and is expected to be a short-term phenomenon and as a result is not expected to be important in U Gem even a week or two after the outburst. However, Godon, et al. (2006) have had difficulty in explaining the slow decline in the temperature of the WD in WZ Sge without ongoing heating of the WD via continued accretion.

Of the well-studied systems, U Gem is unique in that UV flux does not decline as rapidly as expected if the emission arises solely from a uniform temperature WD with fixed radius. This is apparent in the *FUSE* analysis and had been seen previously in HUT and *HST* spectra (Long et al. 1993, 1994). By contrast, similar analyses of WZ Sge show that all of the post-outburst spectra are consistent with a fixed radius Long et al. (2004). Since it seems unlikely on physical grounds that the radius of the WD in U Gem is actually growing during quiescence, alternative explanations are needed. There are four basic escapes from this dilemma: (a) to argue that the temperature of the WD is not uniform, (b) to argue that the WD is partially obscured during the first observation, (c) to argue that there is a separate source that causes the problem, and (d) to argue that the discrepancy is not sufficiently large to worry about at this time.

The main advantage of solutions to the time-variable radius problem that involve the

a non-uniform surface temperature distribution is that it explains why the spectrum qualitatively resembles that expected from WD. The main theoretical challenge of this kind of interpretation is how to credibly create and maintain the asymmetry on the WD surface once the dwarf nova outburst is over, especially since the readjustment of the internal structure of the WD is basically a spherically symmetric process (at least for a slowly rotating WD). Long et al. (1993) suggested two ways to maintain a hotter region of the WD surface: preferential heating of the portion of the WD surface in a boundary layer near the disk plane powered by ongoing accretion and slow release of kinetic energy stored in a rotating accretion belt spun-up during the preceding outburst.

At that time, the importance of compression heating was not recognized as it is today, so Long et al. (1993) assumed that difference in luminosity just after outburst and in midquiescence had to be fully explained. Since the extra luminosity was  $3 \times 10^{32}$  ergs s<sup>-1</sup>, this implied an accretion rate of  $1.7 \times 10^{15}$  g s<sup>-1</sup>, far greater than would have been derived from the X-ray luminosity of  $1.1 \times 10^{31}$  erg s<sup>-1</sup> (Szkody et al. 1996). They were also concerned that if the accretion rate were this high, then observational signatures of the disk should have been seen in the HUT (850-1850 Å) spectra. Today, it is less clear that these specific problems rule out continued accretion as the cause of the distortions in the spectrum of U Gem. However, most of the evidence today is that accretion on the WD is fairly spherical. In particular, while in outburst the boundary layer is thought to be optically thick and geometrically thin,<sup>7</sup> in quiescence the boundary layer is expected to be optically thin and geometrically thick. High resolution X-ray observations of U Gem (Szkody et al. 2002) and other systems show that the X-ray emission arises from material that is not rotating with the inner disk, which suggests that accretion of this gas, if it occurs at all, is close to spherical.

The basic problem with the accretion belt hypothesis is that there has been little or no detailed modeling of this phenomenon since the pioneering work of Kippenhahn & Thomas (1978) and Kutter & Sparks (1989), and (to our knowledge) no modeling of the specific effects resulting from time variable accretion seen in a dwarf nova outburst.<sup>8</sup> The idea of an accretion belt, which was posited to explain aspects of nova explosion, is that the viscosity of WD envelope is low and therefore that material arriving at the WD surface with Keplerian

<sup>&</sup>lt;sup>7</sup>Geometrically thin may be a misnomer for recent calculations by Fisker & Balsara (2005) suggest that the boundary layer in outburst expands to cover a significant fraction of the WD.

<sup>&</sup>lt;sup>8</sup>Piro & Bildsten (2004) have recently discussed a spreading layer that could moves hot recently accreted material from the equator toward the pole. This could cover up to about 10% of the WD surface at the peak of an outburst and could merge into an accretion belt. But the timescale for this spreading layer to remain a distinct entity is quite short, and as they note, unlikely to account for result a multi-temperature WD surface even ten days after the peak of an outburst.

velocities will spin up the outer layers of the WD near the disk plane. The size and extent of the rotating region would be determined by an instability at the interface between the rotating hydrogen-rich accreting material and outer layers of the WD, which would result in an accretion belt extending, according to Kippenhahn & Thomas (1978), about  $\pm 20^{\circ}$  from the disk plane. It is not clear how important accretion belts are in the context of nova explosions (see, e.g. Porter et al. 1998, for a recent discussion). In any event, Long et al. (1993) suggested that the kinetic energy released in this process might be what was observed in U Gem just after outburst. They pointed out that the "smoking gun" for this explanation would be the detection of lines, particularly higher ionization state lines, that clearly showed evidence of rapid rotation.

There have been a number of attempts to model quiescent systems other than U Gem in terms of the WD and a more rapidly rotating second component. For example, Sion et al. (2001) analyzed HST spectra of VW Hyi in quiescence and showed that  $\chi^2_{\nu}$  was improved if the spectra were modeled in terms of a two component WD (or a WD and a rapidly rotating inner disk annulus), better in terms of  $\chi^2_{\nu}$  than in terms of a uniform temperature WD. More recently, Godon et al. (2004) analyzed a quiescent spectrum of VW Hyi obtained with FUSE, in terms of a two-component WD. They found that the spectrum could be fit in terms of one component with a temperature of 23,000 K rotating with  $v \sin(i)$  of 400  ${\rm km~s^{-1}}$  and s second component with a temperature of 50,000 K rotating at 3000  ${\rm km~s^{-1}}$ . This led Godon & Sion (2005) to suggest that an accretion belt had been detected in VW Hyi. But a careful examination of the spectra described in both of the cases above shows that while there is a clear improvement in  $\chi^2_{\nu}$ , the improvements result from small changes in profile shapes of a large set of lines as well as the overall shape of the spectrum. There is no example of which we are aware in which an individual feature that shows rapid rotation is identified, and as a result, we are not convinced that there is evidence for a rapid rotation in a second component to the emission. A totally featureless second component would likely have produced a similar improvement in  $\chi^2_{\nu}$ . This applies to the *FUSE* observations of U Gem also. Furthermore, we see no clear trends in the widths of individual lines with ionization potential or with observation. This is borne out by the fits as well. One might have hoped, as a result of the higher spectral resolution of FUSE (R $\sim$ 12,500) as compared to HUT (300) or HST ( $\sim 1200$  for the U Gem observations), that a rapidly rotating second component might be more apparent. But the best two-component fits do not consistently indicate that the second higher temperature component, if it exists, is rotating more rapidly than the lower temperature portion of the WD surface.

It should be noted at this stage that it would be possible to create a non-rotating belt if most of the light that is observed from the second component to the emission is reradiated. Fisker & Balsara (2005) have carried out simulations of the boundary layer in non-magnetic

CVs, and suggest that there might be a slowly decaying source of emission from the boundary layer just after outburst during the transition to quiescence. They seem to have in mind a source that is directly observable. They also suggest this is a source might fully account for the long-term cooling of the WD, but as we noted if compression heating is operative, this is not necessary. Nevertheless, if there is a hot boundary layer, it is possible that the second component that we do see is light created in the boundary layer that is re-radiated from slowly rotating WD surface.

The second possibility is that the WD photosphere has a uniform surface temperature, but that the WD is partially obscured by the disk just after outburst, but not far from outburst. Meyer & Meyer-Hofmeister (1994) have suggested that the inner disk extends close to the WD surface immediately after outburst, but that the inner disk evaporates in the early portion of the quiescent period. In this context it might be possible to explain a growth in the apparent radius of the WD. Ignoring limb darkening, the fractional reduction in flux from a WD with the "bottom" half of the WD obscured is given by  $1/2 + 1/2 \cos(i)$  where i is the inclination. For an inclination of 65° the flux would be reduced to 71% that of an unobscured WD, and the implied radius would be 84% of the true radius of the WD. The difference in radii in Obs. 1 and Obs. 2 are of order 10%, and therefore obscuration could explain the apparent growth in WD radius.

Despite the fact that the order of magnitude estimate above indicates that obscuration by the disk if it extended to the interior could obscure the lower portion of the WD, we are skeptical that this is the explanation. The portion of the disk that would have to occult the WD would be located within 1 WD radius of WD surface, and this region is the illuminated (if by nothing else) by the full radiation field of an approximately 40,000 K blackbody.

The third possibility in our list is that there is a second source that causes the WD temperature estimate just after outburst to be too high. This could come about if there is a second component which distorts the spectrum at the shortest wavelengths or if the WD models we (and others) have used are simply not adequate to model the spectrum. The WD in U Gem is not that of a normal WD. The matter is being continually accreted on the surface and in the case of Obs. 1., the face has recently been buffeted by the outburst that preceded it. If the temperature were lower than we have estimated, then the normalization would have to increase to match the observed flux. If we were observing the Rayleigh-Jeans tail of the WD spectrum, then the normalization would scale inversely as the temperature; to increase the normalization by 10% would require a temperature decrease of 10%. Model fits in which the normalization was constrained to be 4.5 (5.5)  $\times$  10<sup>-23</sup> sr imply a T<sub>WD</sub>) of 44,000 (40,000) K instead of the value 46,700 K obtained for Obs. 1., when the normalization is not constrained.

Given the uncertainty in the models, the fact that  $\chi^2_{\nu}$  is not close to one for any type of model we explored, and the possibility of a distorting second component in the spectrum, we do not feel the either a change in WD radius or a multi-component temperature on the WD surface is demanded by the data. This is essentially the last in our list of four possibilities. What is needed at this stage is a better set of data with a number of observations taken after a single outburst.

# 4.2. Phase-dependent Absorption

The mid-quiescence spectrum of U Gem shows time-variable absorption. The absorption is greatest near phase 0.7, but is also observed near phase 0.2. Phase-dependent absorption had been reported in the FUV previously in outburst spectra by Froning et al. (2001), but this represents the first time such absorption has been observed in the FUV in quiescence. As is the case of the mid-quiescence spectrum, variability in the outburst spectra was due to changes in relatively narrow (250-800 km s<sup>-1</sup> FWHM) lines from ions such as Si III and S IV. In outburst, the FUV spectra of U Gem and other DNe are dominated by emission from the rapidly rotating inner disk and therefore Froning et al. (2001) argued that the material producing the absorption had to be elevated above the photosphere of the outer disk. Although line depths were largest between phase 0.53 and 0.79, absorption was observed throughout three separate observations of a single outburst. This implies that the absorbing material is not confined to a single azimuthal region of the disk. If this were the case, in quiescence it would certainly be a concern for abundance analysis assuming lines were formed in the photosphere.

Phase-dependent absorption in U Gem has also been observed in X-rays, both in outburst and in quiescence. In their study of U Gem in outburst with EXOSAT Mason et al. (1988) fitted changes in the flux near phase 0.7 in various energy bands as additional absorption due to cold material, equivalent to  $N_H$  of  $3 \times 10^{20}$  cm<sup>-2</sup>. However, the EUVE observations analyzed by Long et al. (1996) indicate that the continuum source is almost fully obscured and the emission that remains are photons scattered by a wind that extends above the surface of a disk which appears thicker at some orbital phases than others. In quiescence, observing with ASCA, Szkody et al. (1996) saw a 50% drop in the 0.5-2 keV X-ray flux near phase 0.7. The absorption was far less at higher energies, and Szkody et al. (1996) concluded that the data were consistent with an X-ray source of order the size of the WD, and extra absorption equivalent to  $N_H$  of  $3.6 \times 10^{21}$  cm<sup>-2</sup> at phase 0.7. This is roughly consistent with the value of  $2 \times 10^{21}$  cm<sup>-2</sup> that we infer from our analysis in Sec. 3.

Phase-dependent absorption in CVs is generally understood to be a consequence of the

interaction between the disk and the stream of material from the secondary star. This is also the explanation for a similar phenomenon in a class of compact low-mass X-ray binaries, known as "X-ray dippers", which also show absorption near orbital phase 0.7. Lubow & Shu (1976) were the first to discuss the possibility that gas flowing over the disk from the secondary would have a vertical scale height substantially larger than the standard scale height of the disk. Frank et al. (1987), in the context of X-ray binaries, were the first to suggest that thickening of the disk near the circularization radius ( $\sim 10^{10}$  cm) rather than at the edge of the disk, and to predict that "dips" rather than full occultations of the central X-ray source should occur in the inclination range 60-75°. In the case of U Gem, Doppler images clearly show a stream penetrating well inside the outer edge of the disk with velocities intermediate between those expected for an unimpeded stream and co-rotation with the disk (Marsh et al. 1990). Hirose et al. (1991) carried out the first 3-D particle simulations of disks, indicating that the ratio of the vertical height of the disk was 10-20\% of the disk radius and is greatest near orbital phases 0.8 and (to a lesser degree) 0.2, which is what we see in the Obs. 2 FUSE data. More recently, Kunze et al. (2001) have carried out SPH-simulations of stream overflow, including cases with the system parameters of U Gem, indicating that a substantial fraction of the material settles at 30-40% of the distance from the WD to inner Lagrange point, an indicating that material can reach altitudes of 20-25° of the disk plane. No one, to our knowledge, has reported the line of sight velocities of the material along the line of sight to the WD. This would be quite interesting, since the FUSE data shows absorption lines that are redshifted by about 120 km s<sup>-1</sup> at between phases 0.6-0.85, and blues shifted by about 50 km s<sup>-1</sup> at phases 0.2-0.35 with respect to the WD.

#### 4.3. CNO-processed material in the WD photosphere

Despite the time variable-absorption that was observed in the Obs. 2 spectra, the fact that fits to both the Obs. 1 and the unabsorbed portion of the Obs. 2 were improved using models with large N overabundances and sub-solar C abundances provides strong support for the existence of CNO processed material in the WD photosphere of U Gem The confirmation using FUSE data of earlier suggestions arising primarily from HST data (Sion et al. 1998; Long & Gilliland 1999) is important because there is only one strong N line in the HST wavelength range, NIII  $\lambda 1184$ .

U Gem was one of the first CVs for which a large N overabundance was suggested based on an analysis of abundances on the surface of the WD, but there is increasing evidence that a significant fraction of CVs exhibit anomalous abundance ratios, and more specifically large N overabundances (see, e. g. Gänsicke et al. 2003). Evidence for CNO processed material

has been reported not only from UV spectra of the WDs in CVs, but also in IR spectroscopy of some CV secondaries (including U Gem, Harrison et al. 2005), and in UV spectra of the disks of some in the form of anomalously large NV:CIV line ratios (Mauche et al. 1997; Gänsicke et al. 2003). This and the fact that heavy elements quickly sink below the WD photosphere (Paquette et al. 1986) suggests that the CNO material on the WD surfaces of CVs is accreted from the secondary. Two sources of this material have been proposed: (a) a secondary that was originally massive and survived the thermal mass transfer stage, possibly leading to a supersoft X-ray stage (Schenker et al. 2002), which is now bringing CNO-enriched material to the surface from the core by convection, and (b) nova-explosions that pollute the atmosphere of the secondary (Marks et al. 1997). At present, it unclear which of these suggestions is correct. Sion et al. (2001) did report the discovery of large overabundances of P and an a general abundance pattern in one HST spectrum of VW Hyi that suggest material from the thermonuclear runaway expected in a nova explosion, but this has not (to our knowledge) been seen in any other system. Furthermore, even if it is correct in this case it is not clear that it could account for the bulk of the systems in which CNO-processed material has been observed.

#### 4.4. Radius and Mass of the WD in U Gem

Long & Gilliland (1999) used 1162-1448 Å HST/GHRS spectra to determine a radius of  $4.7 \pm 0.6 \times 10^8$  cm and inferred from this a WD mass of  $1.14 \pm 0.07$   $M_{\odot}$ . They based their determination on log g=8.5 model estimate of the normalization factor of  $4.11 \times 10^{-23}$  and a distance of  $82\pm13$  pc derived from the Bailey's (1981) method. Using the mid-quescence FUSE spectrum, single temperature, scaled-abundance models,j and a distance of  $100.4\pm3.7$  pc (Harrison et al. 2004), we find a radius of  $5.7^{+0.5}_{-0.2} \times 10^8$  cm. Assuming the WD in U Gem obeys a standard mass-radius relationship (Anderson 1988) and that the surface of the WD is fully visible, the FUSE analysis leads directly to a mass estimate of  $1.00^{+0.04}_{-0.05} M_{\odot}$ , where the error bars here are determined simply by the results of the various gravities in the models.<sup>9</sup> The results are not consistent with one another. Why? The answer is solely that the distance has increased by 22%. Long & Gilliland (1999) used the Bailey (1981) relation to establish the distance of  $82\pm13$  pc for an inclination of  $67^{\circ}$ , whereas we have used the new astrometric distance, which should be more reliable. With the larger distance, the radius derived by Long & Gilliland (1999) would have been  $5.7\pm0.8\times10^8$  cm, almost identical to the values obtained with the FUSE data. This is not surprising since the measured  $T_{WD}$ ,

 $<sup>^9</sup>$ Using Obs. 1, the radius is  $5.1^{+0.2}_{-0.3} \times 10^8$  cm and the mass is  $1.10^{+0.02}_{-0.04}$   $M_{\odot}$ . But the Long & Gilliland (1999) measurement was made in mid-quiescence, as was the case for Obs. 2.

observed fluxes, and indeed the models used to analyses the data are similar.

Naylor et al. (2005) have recently conducted a detailed study of the secondary star in U Gem. They find  $K_2$  to be 300 km s<sup>-1</sup>, very precisely, in agreement with earlier values 309±3 km s<sup>-1</sup> (Friend et al. 1990) and 283±15 km s<sup>-1</sup> (Wade 1981). They also find an accurate value of 29±6 km s<sup>-1</sup> for  $\gamma_2$ , somewhat lower than the value of 46±6 km s<sup>-1</sup>, obtained by Friend et al. (1990), and considerably lower than the value of 84.9±9.9 km s<sup>-1</sup> obtained by Wade (1981). From the value of  $\gamma_1$  for the WD obtained by Long & Gilliland (1999) from the lower ionization-state lines in the GHRS spectra of U Gem, they derive a gravitational redshift  $\gamma_{grav}$  of 143±15 km s<sup>-1</sup>. Based on this determination of for  $\gamma_{grav}$  for the WD, Naylor et al. (2005) concluded that  $R_{WD}$  was, reading directly from Fig. 8 of that paper, 3.9 ± 0.4 × 10<sup>8</sup> cm, if the WD in U Gem obeys the Hamada-Salpeter mass radius relationship (Hamada & Salpeter 1961), or alternatively, 3.7 ± 0.9 × 10<sup>8</sup> cm if the inclination of U Gem between 62 and 74°. The conundrum uncovered by this analysis is the photospheric radius derived from the fits to HST spectra of U Gem corrected to reflect the astrometric distance is about 50% larger than the gravitational radius. The photometric radius 5.7<sup>+0.5</sup><sub>-0.2</sub> × 10<sup>8</sup> cm we derive from FUSE spectroscopy, does not change this picture.

The basic situation is shown in Fig. 12, which is similar to Fig. 8 of Naylor et al. (2005), based on the FUSE results described here. (The slightly higher value of  $K_1$  obtained with FUSE implies a somewhat higher WD mass for a fixed inclination.) For specificity, suppose the actual inclination is  $67^{\circ}$ . Then  $M_{WD}$  is  $1.26\,M_{\odot}$  and  $R_{WD}$ , based on  $\gamma_{grav}$ , should be  $3.8\times10^8$  cm, whereas  $R_{WD}$  inferred from the FUSE spectral analysis of Obs. 2 is  $5.7^{+0.5}_{-0.2}\times10^8$  cm, or 1.5 times larger. This means, since the flux scales with  $R_{WD}^2$ , that the observed flux is 2.3 times larger than expected. This is a large difference. To obtain the observed flux,  $T_{WD}$  for Obs. 2 would have to be increased to  $\sim 38,000$  K, assuming all other aspects of our analysis are correct. The shapes of a the 38,000 K model spectrum is qualitatively different from that observed with FUSE in Obs. 2. It seems very unlikely that this can explain why the radius derived from the spectral analysis is so much larger than predicted from the orbital parameters and  $\gamma_{grav}$ .

Photometric determinations of the radius are crucially dependent on the estimate of distance. Indeed Fig. 7 of Long & Gilliland (1999), which is very similar to our Fig. 12 contains no hint of a difficulty reconciling the photometric radius with that predicted by the Hamada & Salpeter (1961) relationship. It is interesting in this regard that Schreiber & Gänsicke (2002) have had difficulty in explaining the fact that SS Cyg does not show standstills in view of the larger mass transfer rate implied by an upward revision of the distance to SS Cyg based on Harrison et al. (2004). It is possible that the astrometric distance derived by Harrison et al. (2004) is incorrect, although that certainly seems unlikely.

In any event, it would be useful in this regard to have an independent parallax distance for U Gem (and SS Cyg).

Flux-based determinations of  $R_{WD}$  also depend upon the assumption that the synthetic spectra used to compare with data have not only the correct shape, but also the correct surface fluxes. This is an assumption that could be questioned in view of the fact that we generated spectra from very simple pure H, LTE atmospheres. We have, however, performed several tests to assure ourselves that the surfaces fluxes are not significantly affected by the simplicity of our assumption about the structure of the atmosphere. First, we performed tests in which we compered spectra from atmospheres calculated assuming solar abundances to those calculated from H. At the temperatures and gravities appropriate for U Gem, the fractional differences in the surface fluxes were quite small, less than 5% in the FUSEwavelength range. Second, we created a model spectrum for Sirius B using the  $T_{WD}$  and gravity obtained by Barstow et al. (2005). We normalized the spectrum using parallax distance and  $R_{WD}$  for Sirius B. Our model fluxes are within about 15% of the fluxes observed with HST in the wavelength range 1780-1930 Å. Third, to check whether different sets of opacities or a different code might produces a significantly different flux, we compared spectra generated using Tlusty/Synspec with our simple LTE assumptions with Kurucz (1992) model spectra. At temperatures near 30,000 K, we found good agreement between the Kurucz model spectra (which are admittedly for lower gravities) and those generated with TLUSTY/SYNSPEC. In particular, at wavelengths between 1050 and 1700 Å (selected to cover the spectral ranges analyzed here and by Long & Gilliland), the spectra agree in terms of overall normalization to an accuracy of about 20%. Hence, insofar as we can determine, the disagreement between the photometric radius and the gravitational radius is not due to inadequacies in the model spectra being used for the analysis.

If the solution is not in the WD models or the distance, and if the determination of  $\gamma_{grav}$  is correct, then one is left to argue that there is some second source in U Gem. The most obvious possibility is the disk, and, as we have noted, there are some evidence of emission from the disk, in double peaked excesses of emission at the position of the Lyman lines. In SS Cyg and WX Hyi where continuum emission from the disk is seen, emission is accompanied by broad emission lines from resonance lines of N V, Si IV, and C IV (Long et al. 2005). There is no evidence of this in HST spectra of U Gem in quiescence. Aside from the excesses near the Lyman lines, there is no evidence for a rapidly rotating component in U Gem. If the emission arises from the inner disk, the lines widths would be very broad and it is hard to reconcile this with the deep, relatively narrow absorbtion lines observed in the FUSE spectra. The second component would also have to have a spectrum that mimicked that of a WD. In VW Hyi where the FUSE observations show two distinct emission components the second component is most visible at the shortest wavelengths and it does not show the deep

Lyman line profiles of a WD (Godon et al. 2004).

One can of course question the measurements of  $\gamma_{grav}$ , but to bring the photometric radius and gravitational radius into agreement, one would one would need to reduce  $\gamma_{grav}$ , to about 100 km s<sup>-1</sup>. Since  $\gamma_{grav} = \gamma_1 - \gamma_2$ , one can question the determinations of either of  $\gamma_1$  of the WD or  $\gamma_2$  the secondary, or both. Naylor et al. (2005) used their value of  $\gamma_2$ of  $29\pm6$  km s<sup>-1</sup>, which is the lowest of all of the determinations of  $\gamma_2$  in conjunction with the highest value of  $\gamma_1$  of 172.1 $\pm$  15 km s<sup>-1</sup> determined by Long & Gilliland (1999) from low ionization state lines, and the discrepancy of between the photometric radius and the gravitational radius is therefore maximized by the choice. The  $\gamma_1$  of the WD that is derived from the FUSE data is lower than that obtained by Long & Gilliland (1999) and by Sion et al. (1998), but the difference is not nearly enough. Furthermore, even in the absence of the measurement of  $\gamma_{qrav}$ , the photospheric radius appears to be significantly larger than the Hamada-Salpeter mass-radius relationship suggests. (The inclination of U Gem cannot be greater than 74° or it would fully eclipse.) The Hamada-Salpeter relation is calculated for cold WDs, and for lower masses the effects of finite temperature significantly alter the expected radii, but for higher masses this effect is small. At 1.1  $M_{\odot}$  for example, Wood (1995) finds that a 100,000 K C/O core WD is only about 10% larger than a cold WD of the same mass, not enough to account for the radius obtained from the flux, the effective temperature, and the distance.

Therefore, we, like Naylor et al. (2005), do not have a good way to explain away this problem. It is quite possible that a number of factors contribute, which suggests that a number of the observation needs to be repeated.

### 5. Summary

In this study, we have reanalyzed FUSE spectra of U Gem obtained by Froning et al. (2001) at the end of an outburst and performed the first analysis of spectra obtained in mid-quiescence after a different but similar outburst. Our primary goal was to contrast the two sets of spectra in order to learn more about the response of the WD to the outburst. The principle surprise in the analysis of the mid-quiescence spectra was the discovery of large phase-dependent absorption in the spectra, which complicated the analysis of the WD spectra, but which provides additional information about material observed previously at X-ray wavelengths that must be located at large distances from the disk plane. Our main conclusions are as follows:

• Both the post-outburst and mid-quiescence spectra are dominated by the WD, as

had been apparent from earlier observations with HUT and HST. The WD, when the FUSE spectra are analyzed in terms of a uniform temperature WD, appears to cool from 41000-47,000 K, depending on gravity, to about 30,000 K, with higher gravities suggesting higher temperatures. Although multi-temperature WD fits improve the fits in a  $\chi^2_{\nu}$  sense, the data do not require multiple temperatures, especially since none of the fits that we have carried out result in values of  $\chi^2_{\nu}$  approaching a value of 1. There are a variety of alternatives, additional components to the spectrum as well as inadequacies in the WD models, that could explain the apparent deficiencies in the model fits.

- We find a  $K_1$  velocity for the WD of approximately 120 km s<sup>-1</sup>. This is close to but slightly larger than the values deduced by Long & Gilliland (1999) and by Sion et al. (1998). The difference in  $K_1$  only minimally affects the determination of WD mass. There appear to be some differences in the  $\gamma$  velocity derived from different lines, as suggested by the analysis of Long & Gilliland (1999), and our measurement of the  $\gamma$  velocity is somewhat smaller than determined by Long & Gilliland (1999) or Sion et al. (1998).
- The abundance analyses of both the post-outburst and the mid-quiescent spectrum confirm CNO enrichment of the material being accreted onto the WD photosphere. The actual values of the abundances, especially the large overabundances that are found in some cases, are probably suspect, but the basic conclusion is not. In particular, it is clear that one must be concerned about the problem of absorption material within the system.
- The absorbing material that is seen preferentially near phases 0.2 and 0.7 in the midquiescence spectrum is due to ionized material with an effective temperature of 10,000-11000 K if the density of the gas is about 10<sup>13</sup> cm<sup>-3</sup>, a few thousand degrees hotter if the density is 10<sup>9</sup> cm<sup>-3</sup>. The same material is probably also responsible for the absorption seen in X-rays previously.
- Our analysis of the FUSE data reenforces the fact that there is a severe and unexplained discrepancy between the photometric radius derived from the FUV flux observed in mid-quiescence, the temperature derived from spectral fits to the spectrum, and the astrometric distance obtained by Harrison et al. (2004), and the radius inferred from mass determined from  $K_1$ ,  $K_2$ , and either  $\gamma_{grav}$  or the Hamada-Salpeter mass-radius relationship.

This analysis of FUSE data would not have been possible without the financial support from NASA through grants NAG5-9283 and NNG04GQ38G. We appreciate this, as well the dedicated efforts of the entire FUSE team. We also appreciate the efforts of an anonymous referee who made numerous constructive comments on the original manuscript.

### REFERENCES

Ak, T., Ozkan, M. T., & Mattei, J. A. 2002, A&A, 389, 478

Anderson, N. 1988, ApJ, 325, 266

Bailey, J. 1981, MNRAS, 197, 31

Barstow, M. A., Bond, H. E., Holberg, J. B., Burleigh, M. R., Hubeny, I., & Koester, D. 2005, MNRAS, 362, 1134

Cheng, F. H., Sion, E. M., Szkody, P., & Huang, M. 1997, ApJ, 484, L149

Fisker, J. L., & Balsara, D. S. 2005, ApJ, 635, L69

Frank, J., King, A. R., & Lasota, J.-P. 1987, A&A, 178, 137

Friend, M. T., Martin, J. S., Connon-Smith, R., & Jones, D. H. P. 1990, MNRAS, 246, 637

Froning, C. S., Long, K. S., Drew, J. E., Knigge, C., & Proga, D. 2001, ApJ, 562, 963

Gänsicke, B. T., & Beuermann, K. 1996, A&A, 309, L47

Gänsicke, B. T., et al. 2003, ApJ, 594, 443

Godon, P. & Sion, E. M. 2002, ApJ, 566, 1084

Godon, P., & Sion, E. M. 2005, MNRAS, 361, 809

Godon, P., Sion, E. M., Cheng, F., Long, K. S., Gänsicke, B. T. & Szkody, P. 2006, ApJ, submitted

Godon, P., Sion, E. M., Cheng, F. H., Szkody, P., Long, K. S., & Froning, C. S. 2004, ApJ, 612, 429

Hamada, T. & Salpeter, E. E. 1961, ApJ, 134, 683

Hameury, J., Lasota, J., & Warner, B. 2000, A&A, 353, 244

Harrison, T. E., Johnson, J. J., McArthur, B. E., Benedict, G. F., Szkody, P., Howell, S. B., & Gelino, D. M. 2004, AJ, 127, 460

Harrison, T. E., Osborne, H. L., & Howell, S. B. 2005, AJ, 129, 2400

Hirose, M., Osaki, Y., & Mineshige, S. 1991, PASJ, 43, 809

Horne, K., Marsh, T. R., Cheng, F. H., Hubeny, I., & Lanz, T. 1994, ApJ, 426, 294

Hōshi, R. 1979, Progress of Theoretical Physics, 61, 1307

Hubeny, I. 1988, Comput. Phys. Comm., 52, 103

Hubeny, I. & Lanz, T. 1995, ApJ, 439, 875

Kiplinger, A. L., Sion, E. M., & Szkody, P. 1991, ApJ, 366, 569

Kippenhahn, R. & Thomas, H.-C. 1978, A&A, 63, 265

Kriss, G. 1994, ASP Conf. Ser. 61: Astronomical Data Analysis Software and Systems III, 61, 437

Kunze, S., Speith, R., & Hessman, F. V. 2001, MNRAS, 322, 499

Kurucz, R. L. 1992, IAU Symp. 149: The Stellar Populations of Galaxies, ed. B. Barbuy & A. Renzini (Dordrecht:Kluwer), 149, 225

Kutter, G. S., & Sparks, W. M. 1989, ApJ, 340, 985

Lampton, M., Margon, B., & Bowyer, S. 1976, ApJ, 208, 177

Long, K. S., Blair, W. P., Bowers, C. W., Davidsen, A. F., Kriss, G. A., Sion, E. M., & Hubeny, I. 1993, ApJ, 405, 327

Long, K. S., Blair, W. P., & Raymond, J. C. 1995, ApJ, 454, L39

Long, K. S., Froning, C. S., Gänsicke, B., Knigge, C., Sion, E. M., & Szkody, P. 2003, ApJ, 591, 1172

Long, K. S., Froning, C. S., Knigge, C., Blair, W. P., Kallman, T. R., & Ko, Y.-K. 2005, ApJ, 630, 511

Long, K. S. & Gilliland, R. L. 1999, ApJ, 511, 916

Long, K. S., Mauche, C. W., Raymond, J. C., Szkody, P., & Mattei, J. A. 1996, ApJ, 469, 841

Long, K. S., Sion, E. M., Gänsicke, B. T., & Szkody, P. 2004, ApJ, 602, 948

Long, K. S., Sion, E. M., Huang, M., & Szkody, P. 1994, ApJ, 424, L49

Lubow, S. H., & Shu, F. H. 1976, ApJ, 207, L53

Lynden-Bell, D. & Pringle, J. E. 1974, MNRAS, 168, 603

Marks, P. B., Sarna, M. J., & Prialnik, D. 1997, MNRAS, 290, 1977

Mauche, C. W., Lee, Y. P., & Kallman, T. R. 1997, ApJ, 477, 832

Marsh, T. R., Horne, K., Schlegel, E. M., Honeycutt, R. K. & Kaitchuck, R. H. 1990, ApJ, 364, 637

Mason, K. O., Cordova, F. A., Watson, M. G., & King, A. R. 1988, MNRAS, 232, 779

Mineshige, S. & Osaki, Y. 1983, PASJ, 35, 377

Meyer, F., & Meyer-Hofmeister, E. 1994, A&A, 288, 175

Moos, H. W. et al. 2000, ApJ, 538, L1

Naylor, T., Allan, A., & Long, K. S. 2005, MNRAS, 361, 1091

Panek, R. J. & Holm, A. V. 1984, ApJ, 277, 700

Paquette, C., Pelletier, C., Fontaine, G., & Michaud, G. 1986, ApJS, 61, 197

Piro, A. L., Arras, P., & Bildsten, L. 2005, ApJ, 628, 401

Piro, A. L., & Bildsten, L. 2004, ApJ, 610, 977

Porter, J. M., O'Brien, T. J., & Bode, M. F. 1998, MNRAS, 296, 943

Pringle, J. E. 1988, MNRAS, 230, 587

Schenker, K., King, A. R., Kolb, U., Wynn, G. A., & Zhang, Z. 2002, MNRAS, 337, 1105

Sahnow, D. J. et al. 2000, ApJ, 538, L7

Schreiber, M. R., Gänsicke, B. T. 2002, A&A, 382, 124

Seaton, M. J. 1979, MNRAS, 187, 73P

Sion, E. M. 1995, ApJ, 438, 876

Sion, E. M., Cheng, F. H., Gänsicke, B., Sparks, W. M., & Hubeny, I. 2001, ApJ, 561, L127

Sion, E. M., Cheng, F. H., Szkody, P., Sparks, W., Gänsicke, B., Huang, M., & Mattei, J. 1998, ApJ, 496, 449

Sion, E. M., Cheng, F.-H., Szkody, P., Gänsicke, B., Sparks, W. M., & Hubeny, I. 2001, ApJ, 561, L127

Szkody, P. & Mattei, J. A. 1984, PASP, 96, 988

Szkody, P., Long, K. S., Sion, E. M., & Raymond, J. C. 1996, ApJ, 469, 834

Szkody, P., Nishikida, K., Raymond, J. C., Seth, A., Hoard, D. W., Long, K. S., & Sion, E. M. 2002, ApJ, 574, 942

Townsley, D. M., & Bildsten, L. 2002, ApJ, 565, L35

Verbunt, F. 1987, A&AS, 71, 339

Wade, R. A. 1981, ApJ, 246, 215

Wood, M. A. 1995, LNP Vol. 443: White Dwarfs, 443, 41

This preprint was prepared with the AAS LATEX macros v5.2.

- Fig. 1.— Optical lightcurves of U Gem at the time of the *FUSE* observations using data assembled by the AAVSO (E. O. Waagen 2004, private communication).
- Fig. 2.— The FUSE spectra of U Gem obtained during Obs. 1 (black) shortly after outburst and Obs. 2 (grey) when the system was far from outburst with the lines labeled. Most of the lines observed in Obs. 1 also appear in Obs. 2, including some high ionization lines, e.g. O VI  $\lambda\lambda 1032, 1038$ .
- Fig. 3.— The upper panel shows the normalized flux in the wavelength range 1045-1055 Å from U Gem in Obs. 2 as a function of orbital phase. The phase intervals that were used to construct the "unabsorbed" spectrum are shown in black. The lower panel shows the "unabsorbed" spectrum in black and the spectrum obtained during phase intervals 0.6 to 0.85 in grey. The 0.1 A spectra were smoothed with a 0.5 A boxcar to create this figure. below.
- Fig. 4.— Uniform temperature solar abundance WD model fits to the Obs. 1 spectrum. The data are plotted in grey; the best log g = 8.5 model, with abundances that were individual varied is plotted in blue. For comparison, the best fit model assuming log g = 8.5 and solar abundances is plotted in red The regions of the data that were excluded from the fitting are shown in a lighter shade of grey. The positions of various lines are indicated. Lines that are clearly seen in the spectrum are indicated by thicker labels. The narrow emission feature centered on Lyman $\beta$  is due to airglow.
- Fig. 5.— Uniform temperature WD model fit to the Obs. 2 spectrum. The format of the figure is identical to that of Fig. 4. The best fit model assuming log g = 8.5 and solar abundances is plotted in red. The best fit when individual abundances of was allowed to vary is plotted in blue. The narrow emission feeatures at Lyman $\beta$  and Lyman $\gamma$  are due to airglow.
- Fig. 6.— A two-T log g=8.5 fit to the Obs. 1 spectrum of U Gem. The data and the model fit are shown as in the previous figures. In addition, the contribution of the low and higher temperature components are shown as the dotted and dashed lines, respectively. The higher temperature component dominates throughout, but especially at the shortest wavelengths.
- Fig. 7.— Similar to Fig. 6, except for a model consisting of a WD and a powerlaw second component.
- Fig. 8.— A comparison of spectra obtained during Obs. 2 that we have called "unabsorbed" (black) compared to the that observed during Phase 0.2-0.35 (red) and Phase 0.6-0.85 (blue).

Fig. 9.— Attempts to fit the spectra during the "absorbed" phase of Obs. 2 with an LTE slab absorbing the light of the WD. The upper, middle, and lower panels show fits to the "Unabsorbed", phase 0.2-0.35, and phase 0.6-0.85 spectra, respectively. The data are plotted in grey and regions that were excluded in a lighter grey. The solid red line corresponds to the fit obtained assuming that a slab of material lies along the line of sight to a WD with log g of 8.5 and solar abundances. The solid green line is the WD with the absorption removed. Although only a 100 Å region from 1078-1178 Å region is shown, the fit was based on the entire spectrum.

Fig. 10.— Radial velocity fits to the FUV spectra of U Gem. The upper panel shows the velocity shifts of the Obs. 1 spectrum vs. orbital phase with the best fit radial velocity curve with an amplitude of  $122\pm10~{\rm km\,s^{-1}}$ . The lower panel shows the velocity shifts of the Obs. 2 spectrum and the best fit radial velocity curve, with an amplitude of  $132\pm6~{\rm km\,s^{-1}}$ ; if the portions of the data obtained during phases 0.2-0.35 and 0.6-0.85 are excluded the best fit value of  $K_1$  in Obs. 2 drops to  $117^{+9}_{-8}~{\rm km\,s^{-1}}$ . In both panels, the velocity shifts of the Si IV 1128 Å line with open triangles. In the lower plot, the shifts of the Si III  $\lambda 1110$  and 1113 Å lines are plotted with open squares and open circles, respectively.

Fig. 11.— Selected regions of the spectra obtained from the LiF1 channel for Obs. 1 and 2. The spectra plotted in black have orbital motion, here assumed to be 120 km s<sup>-1</sup> removed; the spectra plotted in red are the original unshifted spectra. Lines are labeled assuming  $\gamma_1$  of 110 km s<sup>-1</sup>. A shift of 100 km s<sup>-1</sup> corresponds to 0.37 Å at these wavelengths.

Fig. 12.— Constraints on the mass and radius of the WD in U Gem for a  $K_1$  velocity of 120 km s<sup>-1</sup> and  $K_2$  velocity of 300 km s<sup>-1</sup>. Constraints imposed for various values of the gravitational redshift are shown; the black lines are the values and errors derived by Naylor et al. (2005), using the Long & Gilliland (1999) value for  $\gamma_1$  and their value of  $\gamma_2$ . The grey lines are similar, but use the average $\gamma_1$  from the *FUSE* analysis. The solid black curve, labeled H-S, is the Hamada-Salpeter mass radius relationship. The vertical dashed curves indicate the mass for various inclinations. The horizontal long-dashed lines is the range of photometric radii allowed by single temperature, variable-z fits to Obs. 2. and the astrometric distance to U Gem

Table 1. Observation Log

Obs#	FUSE ID	Date	Start (UT)	End (UT)	Exptime (s)	Days since peak
1	A126	17 Mar 2000		20:34:16	12975	$\sim 10$
2	P154	22-23 Feb 2001		09:08:52	13000	$\sim 135$

Table 2. Uniform Temperature Solar-abundance WD Fits

Obs.	$\log(g)$	Norm $(10^{-23})$	$\frac{R}{(10^8 cm)}$	T (K)	$v \sin(i) $ $( \text{km s}^{-1})$	$\chi^2_{\nu}$
1	8.0	3.7	5.3	40.7	163	7.2
1	8.5	3.3	5.0	43.6	152	6.7
1	9.0	3.0	4.8	47.1	135	6.5
2	8.0	4.3	5.7	28.6	96	7.0
2	8.5	3.4	5.1	30.3	90	6.8
2	9.0	3.1	4.8	31.6	83	7.0

 ${\it Table 3.} \quad {\it Uniform Temperature Variable Z WD Fits}$ 

Obs.	log(g)	Norm $(10^{-23})$	$R \\ (10^8 cm)$	T (1000 K)	Z	$v \sin(i) $ $( \text{km s}^{-1})$	$\chi^2_{\nu}$
1	8.0	4.0	5.3	40.6	1.3	170	7.1
1	8.5	3.3	5.1	43.5	1.4	160	6.7
1	9.0	3.0	4.8	46.8	1.5	148	6.4
2	8.0	5.1	6.2	28.3	3.3	140	6.3
2	8.5	4.3	5.7	29.7	3.9	130	6.0
2	9.0	3.9	5.5	30.9	4.7	116	5.9

Table 4. Multi-Temperature WD Fits

Obs.	$\log(g)$	$ Norm_1 $ $ (10^{-23}) $			$v \sin(i)_1  (km s-1)$		$T_2$ (1000 K)		$v \sin(i)_2  (km s-1)$	$\chi^2_{\nu}$
1	8.0	6.5	26.1	1.5	133	1.1	65.8	9.1	236	5.5
1	8.5	4.5	28.5	1.5	87	1.0	70.0	8.9	243	5.6
1	9.0	3.0	31.0	10.0	186	1.4	60.7	0.8	79	5.7
2	8.0	7.0	25.0	4.3	150	0.6	38.1	3.8	65	5.6
2	8.5	4.6	26.1	5.7	159	1.1	34.5	3.4	76	5.7
2	9.0	3.2	28.8	10.0	139	1.2	33.9	1.7	71	5.8

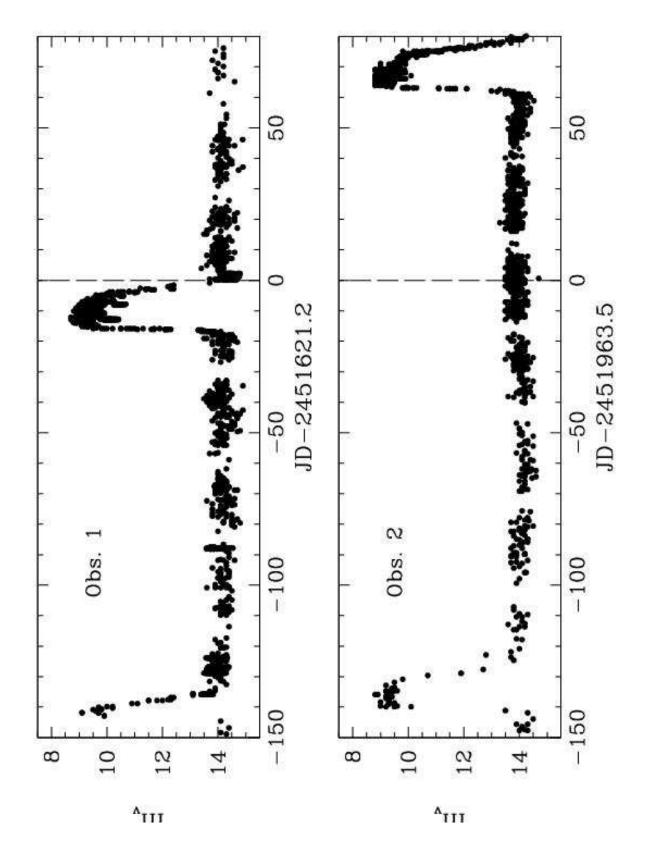
Table 5. WD & Absorbing Screen Fits of Obs. 2

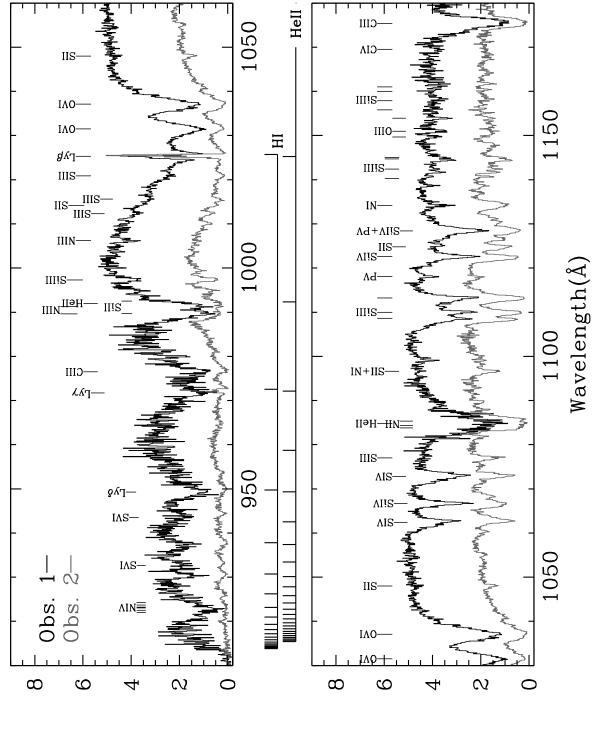
Spectrum	Norm $(10^{-23})$		$v \sin(i) $ $( \text{km s}^{-1} )$	$\frac{\log (NH)}{(cm^{-2})}$	$T_{abs}$ (1000 K)	$v_{abs} (\text{km s}^{-1})$	$\chi^2_{\nu}$ a
Unabsorbed	3.6	30.4	54	19.6	16.8	170	3.4
Phase 0.2-0.35	4.5	29.4	96	20.7	10.3	250	3.4
Phase 0.6-0.85	3.3	29.9	55	21.3	12.0	160	3.1

 $<sup>^{\</sup>mathrm{a}}\mathrm{See}$  text for discussion of  $\chi^{2}_{\nu}$  in these fits.

Table 6.  $\gamma$  Velocities of Selected Lines

Transition	Laboratory Wavelength (Å)	Obs. 1 $\gamma$ ( km s <sup>-1</sup> )	Obs. 2 $\gamma$ ( km s <sup>-1</sup> )
S IV $\lambda$ 1062	1062.662	167	135
Si IV $\lambda$ 1067	1066.6498	151	125
S IV $\lambda$ 1073	1072.974	147	123
Si III $\lambda$ 1108	1108.3579	149	152
Si III $\lambda$ 1110	1109.9696	118	132
Si III $\lambda$ 1113	1113.2296	136	119
Si IV $\lambda$ 1122	1122.4849	146	132





Flux (10-13 ergs cm<sup>-2</sup>  $s^{-1}$  Å<sup>-1</sup>)

